Regulatory T-cells in multiple sclerosis produce IL-10 in the central nervous system but are activated by Epstein-Barr Virus

Running title: EBV Activates Tregs to Produce IL-10 in Multiple Sclerosis

N. Pulvirenti[1], C. Righetti[1], F. Clemente[1], B. Serafini[2], C. Cordiglieri[1], C. Vasco[1], S. Maioli[1,7], A. Pietroboni[3], E. Galeota[1], B. Rosicarelli[2], C. Iannone[8,9], M. de Riz[3], A. Espadas de Arias[4], T. De Feo[4], L. Valenti[5,6], D. Prati[6], S. Abrignani[1,7], M. Gerosa[7,8], R. Caporali[8,9], D. Galimberti[3,9], E. Scarpini[3,9], J. Geginat[1,7]

1 Fondazione Istituto Nazionale di Genetica Molecolare, Milan, Italy

2 Department of Neuroscience, Istituto Superiore di Sanità, Rome, Italy

3 Neurology-Neurodegenerative Diseases Unit, Fondazione IRCCS Ca' Granda Ospedale Maggiore Policlinico, Milan, Italy

4 Laboratorio di Immunologia dei Trapianti - S.C. Trapianti Lombardia-NITp - Fond. IRCCS Cà Granda Ospedale Maggiore Policlinico, Milan, Italy

5 Department of Pathophysiology and Transplantation, Università degli Studi di Milano, Italy

6 Transfusion Medicine, Fondazione IRCCS Ca' Granda Ospedale Maggiore Policlinico, Milano, Italy

7 Department of Clinical Sciences and Community Health, Università degli Studi di Milano, Italy

8 Centro Specialistico Ortopedico Traumatologico Gaetano Pini - CTO, Milan, Italy

9 Department of Biomedical, Surgical and Dental Sciences, Università degli Studi di Milano, Italy

Corresponding author:

Jens Geginat

Via Francesco Sforza, 35, 20122 Milan, Italy, +39 02 00660206, geginat@ingm.org

Abstract

Regulatory T-cells (Tregs) maintain immune homeostasis, but antigens activating adaptive Tregs in human pathologies are ill-defined. EOMES$^+$type-1 regulatory (Tr1)-like T-cells had a dysregulated homeostasis in multiple sclerosis (MS), which was related to their activation in the central nervous system (CNS). EOMES$^+$Tr1-like cells were enriched and clonally expanded in patient's cerebrospinal fluid (CSF) and were the major IL-10-producing T-cell subset in the CNS. Regulatory T-cells from PwMS produced IL-10 and IFN-γ with antigens derived from Epstein-Barr Virus (EBV), but not from myelin. EOMES$^+$Tr1-like cells responded selectively to the latency-associated antigen EBNA1, whereas FOXP3$^+$Tregs and Th1-cells responded also to lytic EBV antigens. EBNA1-specific EOMES$^+$Tr1-like cells were present in patients carrying the HLA-DRB1*15:01 risk allele, were associated with anti-EBNA1 IgG and disappeared upon therapeutic B-cell depletion. IL-10$^+$EOMES$^+$Tr1-like were present in MS brain lesions, and some were in the vicinity of EBV-infected B-cells and CD8$^+$T-cells. Notably, EOMES$^+$Tr1-like cells suppressed CD8$^+$T-cell activation by EBV-infected B-cells. We propose that the insufficient protective functions of Tregs in MS are due to their aberrant anti-viral specificities that promote immune escape of a disease-associated virus.

46 **Introduction**

47 Natural regulatory T-cells (Tregs) are generated in the thymus, express the transcription
48 factor FOXP3 and are required to prevent autoimmunity (Ochs et al., 2007; Sakaguchi et al.,
49 2006). A reduced number or functionality of FOXP3^{+}Tregs to control the activation of
50 autoreactive T-cells is therefore thought to play a crucial role in autoimmune diseases
51 (Buckner, 2010). FOXP3^{+}Tregs can however also be generated in the periphery in response to
52 foreign antigens, which may be derived from pathogens (Suffia et al., 2006). Some regulatory
53 T-cells lack FOXP3 expression but produce high levels of the anti-inflammatory cytokine IL-10
54 (Roncarolo et al., 2006). These IL-10 producing "type 1 regulatory T (Tr1)-cells" are adaptive
55 Tregs, which are generated in the periphery in response to self- or foreign antigens (Haringer
56 et al., 2009; Parish et al., 2014), and require thus TCR stimulation by specific antigens for their
57 functions (Gagliani et al., 2010). Tr1-cells are highly heterogeneous (Brockmann et al., 2018).
58 They may produce IL-10 alone or together with IFN-γ (Anderson et al., 2007; Jankovic et al.,
59 2007; Jeon et al., 2012; O'Garra and Vieira, 2007) and inhibit excessive immune responses
60 and immunopathology (O'Garra and Vieira, 2007). During persistent viral infections, IL-10 and
61 IFN-γ co-producing Tr1-like cells are generated upon chronic antigenic stimulation and inhibit
62 collateral tissue damage, but also viral clearance (Murata et al., 2021; Parish et al., 2014). In
63 an increasing number of pathologies, including chronic viral infections, IL-10 and IFN-γ co-
64 producing Tr1-like cells were reported to express the transcription factor EOMESODERMIN
65 (EOMES) and the cytotoxic molecule Granzyme-K (GzmK) (Bonnal et al., 2021; Geginat et al.,
66 2023; Gruarin et al., 2019; Haringer et al., 2009; Thelen et al., 2023; Zhang et al., 2017). Similar
67 to FOXP3^{+}Tregs, EOMES^{+}Tr1-like cells can suppress CD8^{+}T-cell responses (Bonnal et al., 2021;
68 Pulvirenti et al., 2024), the key effector cells that control viral infections. Not all EOMES-
69 expressing CD4^{+}T-cells are however Tr1-like cells, since those expressing CCR6 or GzmB have
70 pro-inflammatory properties (Dejean et al., 2019; Mazzoni et al., 2018; Pulvirenti et al., 2024).
71 However, pro-inflammatory EOMES^{+}Th1-cells may differentiate to anti-inflammatory
72 EOMES^{+}Tr1-like cells upon chronic antigenic activation in a negative feedback loop to inhibit
73 immunopathology (Gabrysova et al., 2009; Geginat et al., 2023; O'Garra and Vieira,
74 2007)(Zhang, Immunity, 2025).

75 Multiple sclerosis (MS) is the most common chronic inflammatory demyelinating disease of
76 the central nervous system (CNS) with a prevalent relapsing-remitting (RR-MS) onset that can

77 evolve into a progressive course (P-MS). The aetiology is still unclear, but both genetic and
78 environmental factors contribute critically to the overall disease risk (Olsson et al., 2017). The
79 strongest genetic risk factor is the human leukocyte antigen (HLA) class II allele HLA-
80 DRB1*15:01 which encodes an MHC class 2 molecule that could present critical self-peptides
81 to activate autoreactive $CD4^+$T-cells (Wang et al., 2020). Among environmental factors,
82 infection with the almost ubiquitous herpesvirus Epstein-Barr Virus (EBV) is a necessary,
83 although not sufficient, condition for initiating inflammatory brain damage leading to MS
84 (Bjornevik et al., 2023). EBV-associated infectious mononucleosis and anti-Epstein Barr Virus
85 nuclear antigen (EBNA)1 IgG levels interact with HLA-DRB1*15:01 to increase the risk of MS.
86 However, the mechanism by which EBV promotes MS is still a focus of intense research (Aloisi
87 et al., 2023; Christensen, 2006; Geginat et al., 2017; Murata et al., 2021). Accumulating
88 evidence indicates an altered immune response to EBV in MS, and anti-EBV immune
89 surveillance may be inefficient in MS (Geginat et al., 2017; Kuchroo and Weiner, 2022).
90 Regulatory T-cells are thought to be reduced or defective in MS, since they fail to prevent CNS
91 damage. MS-like disease symptoms were however not reported in FOXP3-deficient mice or
92 patients (Ochs et al., 2007), and reduced $FOXP3^+$Treg numbers are not consistently associated
93 with MS (Noori-Zadeh et al., 2016). $FOXP3^+$Tregs proliferate however less upon TCR
94 stimulation in MS (Carbone et al., 2014), produced higher amounts of IFN-γ and lower
95 amounts of IL-10, and may thus be functionally impaired (Dominguez-Villar et al., 2011;
96 Sumida et al., 2018). Tr1-like cells producing IL-10 and IFN-γ were shown to play a protective
97 role in experimental autoimmune encephalomyelitis (EAE), a widely used animal model of
98 autoimmunity-driven CNS inflammation (Heinemann et al., 2014). Moreover, the generation
99 of IL-10 producing $CD4^+$T-cells *in vitro* was defective in MS (Astier et al., 2006), suggesting that
100 the differentiation of potentially protective Tr1-cells may be impaired. However, if
101 $EOMES^+$Tr1-like cells are involved in MS or anti-EBV immune control is unknown (Geginat et
102 al., 2023). Notably, EOMES expression in $CD4^+$T-cells promoted CNS inflammation in EAE
103 (Stienne et al., 2016), suggesting that pro-inflammatory $EOMES^+$T-cells could promote CNS
104 damage. Moreover, cytotoxic $CD4^+EOMES^+GzmB^+$T lymphocytes (CTL) were proposed to play
105 a pathogenic role in MS (Peeters et al., 2017; Raveney et al., 2021). Here, we investigated the
106 features of $CD4^+EOMES^+$T-cell subsets in MS. We found that $EOMES^+$Tr1-like cells were
107 activated *in vivo,* produced high amounts of IL-10, accumulated and were clonally expanded

108 in the CNS. However, they were specific for the EBV-derived antigen EBNA1, suggesting that
109 they are insufficient to prevent CNS autoimmune damage and promote EBV immune escape.

110 **Results**

111 **The homeostasis of EOMES$^+$Tr1-like cells is dysregulated in MS.**

112 T-cells from peripheral blood (PB) of recently diagnosed, treatment-naive RR-PwMS and age
113 and sex-matched healthy donors (HDs, Table 1) were monitored by multidimensional flow
114 cytometry. Bioinformatic analysis based on unsupervised clustering and dimensionality
115 reduction algorithm, identified 27 T-cell clusters, including 12 CD4$^+$ clusters (Figure 1A, sFigure
116 1). Cluster 11 displayed the phenotype of EOMES$^+$Tr1-like cells (i.e. CD4$^+$EOMES$^+$GzmK$^+$
117 CCR5$^+$PD1$^+$CD27$^+$CCR6$^-$ (Alfen et al., 2018; Geginat et al., 2023; Gruarin et al., 2019)), and co-
118 clustered with CD4$^+$EOMES$^+$T-cells that expressed GzmK and CCR6 (Cluster (Cl) 10, sFigure 1C).
119 In the Uniform Manifold Approximation and Projection (UMAP) maps (Figure 1A) these two
120 GzmK$^+$CD4$^+$T-cell clusters were positioned in the centre of Th1-like clusters (Cl 5,6,8) and
121 CD4$^+$GZMB$^+$CTL (Cl 12), consistent with an intermediate differentiation stage (De Simone et
122 al., 2021; Pulvirenti et al., 2024). Surprisingly, we detected however no major changes in the
123 composition of the T-cell compartments of PwMS and HDs (sFigure 1D).

124 We therefore analysed EOMES$^+$CD4$^+$T-cell subsets more precisely by manual gating in a higher
125 number of subjects, exploiting an established gating strategy (Cossarizza et al., 2021; Gruarin
126 et al., 2019). Thus, we distinguished CD4$^+$EOMES$^+$ subsets according to the expression of
127 GzmB ("CD4$^+$CTL") or GzmK from FOXP3$^+$Tregs and helper T-cells ("Th"), which lack FOXP3 and
128 Granzyme expression (sFigure 2A, B). CD4$^+$GzmK$^+$T-cells were further subdivided into pro-
129 inflammatory GzmK$^+$CCR6$^+$ cells and two Tr1-containing GzmK$^+$CCR6$^-$ populations that
130 expressed different levels of IL-7R. These subsets displayed characteristic cytokine profiles in
131 PwMS (sFigure 2C), as we previously reported in HDs (Pulvirenti et al., 2024). Notably, IL-
132 7R^{lo}GzmK$^+$T-cells had a mature Tr1 profile, since they possessed the highest IL-10 producing
133 capacities but had a low capacity to up-regulate CD40L (sFigure 2C). We then analysed the
134 frequencies and the *in vivo* activation state of T-cell subsets according to the expression of
135 the early activation marker CD69 and the proliferation marker Ki67 *ex vivo* (Figure 1B, sFigure
136 3A). IL-7R^{lo}Tr1-like cells were significantly reduced in PwMS and expressed higher levels of
137 CD69 and Ki67 in RR-PwMS, indicating an increased *in vivo* turnover (Figure 1B). Also IL-
138 7R$^+$Tr1-like cells (sFigure 3A), CD4$^+$CTL and FOXP3$^+$Tregs expressed increased levels of CD69
139 in RR-MS, but their frequencies and *in vivo* turnover rates were not significantly altered. Pro-
140 inflammatory CCR6$^+$GzmK$^+$ cells were in contrast increased in RR-MS but maintained low CD69
141 and Ki67 expression (Figure 1B). Finally, Th-cells represented consistently the large majority

142 of CD4$^+$T-cells and remained largely CD69$^-$ and quiescent in PwMS (sFigure 3A). Thus, only IL-
143 7R^{lo}Tr1-like cells had an increased proliferation in PwMS and were significantly decreased.
144 However, in Natalizumab-treated PwMS frequencies and *in vivo* turnover rates of IL-7R^{lo}Tr1-
145 like cells were similar to those from HDs. Moreover, CD69 expression on all EOMES$^+$Tr1-cells,
146 as well as on FOXP3$^+$Tregs and CD4$^+$CTL, was significantly reduced in Natalizumab-treated as
147 compared to untreated RR-PwMS (Figure 1B, sFigure 3A). Since Natalizumab blocks the
148 adhesion receptor VLA-4 and consequently lymphocyte homing to the CNS, these finding
149 suggested that the altered Tr1 homeostasis in MS is related to CNS homing (Kivisakk et al.,
150 2009). Consistently, the majority of EOMES$^+$Tr1-like cells, as well as of CCR6$^+$GzmK$^+$ cells and
151 of CD4$^+$CTL, expressed VLA-4 in HDs and in PwMS (Figure 1C), suggesting that all cytotoxic
152 CD4$^+$T-cell subsets possess a constitutive high CNS homing potential and can be efficiently
153 targeted by Natalizumab. Conversely, only minor fractions of FOXP3$^+$Tregs and Th-cells were
154 VLA-4$^+$. Moreover, most EOMES$^+$Tr1-cells and CCR6$^+$GzmK$^+$ cells expressed also CXCR3 (Figure
155 1C), a chemokine receptor that is involved in CNS homing in PwMS (Geginat et al., 2017;
156 Kendirli et al., 2023). Notably, CD4$^+$CTL, FOXP3$^+$Tregs and Th-cells expressed significantly
157 lower levels of CXCR3. Furthermore, also most recently divided Ki67$^+$Tr1-like cells were
158 CXCR3$^+$, whereas CXCR3 expression on GZMK$^-$Ki67$^+$T-cell subsets was significantly lower
159 (sFigure 3D).
160 Overall, these findings indicate that the homeostasis of EOMES$^+$Tr1-like cells is dysregulated
161 in MS and suggest that this alteration may be related to CNS homing.
162
163 **Clonally expanded EOMES$^+$Tr1-like accumulate in the cerebrospinal fluid of PwMS.**
164 In order to investigate if EOMES$^+$Tr1-like cells could be recruited to the CNS in PwMS, we
165 interrogated a single cell RNA and TCR sequencing dataset of antigen-experienced CD4$^+$T-cells
166 from paired CSF and blood samples of untreated PwMS and control donors with idiopathic
167 intracranial hypertension (IIH)(Kendirli et al., 2023). To avoid any bias, we adopted the
168 reported bioinformatic strategy and regenerated the same UMAPs (Figure 2A). Considering
169 all differentially expressed genes (DEGs) in the 13 clusters (sTable 1), as well as selected
170 subset-associated marker genes (sFigure 4A-C), we annotated clusters containing cTFH (Cl 1),
171 T_{CM} (CL 2), cells with an type-1 IFN signature (Cl 3), Th17-cells (Cl 4), GzmK^{lo}Th1-like cells (Cl
172 8), Th2-cells (Cl 10) CD4$^+$CTL (Cl12) and FOXP3$^+$Tregs (Cl13) Figure 2A). Clusters 5, 6 and 9
173 lacked a clear gene signature and were annotated as T_{EM}A, B and C. Cluster 7 displayed the

174 gene signature of EOMES$^+$Tr1-like cells (Bonnal et al., 2021; De Simone et al., 2021; Gruarin
175 et al., 2019), as evidenced by a highly significant Gene Set Enrichment Analysis (GSEA, Figure
176 2B). Indeed, several key EOMES$^+$Tr1-like signature genes, namely EOMES (Gruarin et al., 2019)
177 (Figure 2C), CHI3L2 (Bonnal et al., 2021), CCL4, CCR5 and PDCD1 (PD1) (Alfen et al., 2018)
178 were selectively expressed in this cluster (sFigure 4C). Moreover, they expressed the highest
179 levels of GzmK, low levels of IL-7R and lacked CCR6 (Figure 2A, sFigure 4C). Also cells in Cluster
180 11 expressed GzmK and EOMES, but in contrast to Tr1-like cells they expressed CCR6 and high
181 levels of IL-7R (Figure 2D), suggesting that this cluster contained pro-inflammatory
182 CCR6$^+$GzmK$^+$ cells (sFigure 2). The CCR6$^+$GzmK$^+$ cluster was separated in the UMAP from
183 EOMES$^+$Tr1-like cells by a GzmK^{lo}Th1-like cluster (Cl 8, Figure 2A), suggesting that they had
184 largely diverse gene expression patterns. Indeed, cells in the CCR6$^+$GzmK$^+$ cluster expressed
185 lower levels of EOMES$^+$Tr1-like signature genes but very high levels of genes characteristic for
186 pro-inflammatory Th1/17-cells (Figure 2E, sFigure 4C, sTable 2). Notably, the EOMES$^+$Tr1-like
187 cluster in the CSF of PwMS expressed the highest levels of EOMES$^+$Tr1-like signature genes
188 (Figure 2E). They had also an altered expression of genes regulating cholesterol metabolism,
189 but this was a general feature of CSF-infiltrating CD4$^+$T-cells (sTable 3, sFigure 5A)(Hrastelj et
190 al., 2021).
191 Importantly, exclusively the EOMES$^+$Tr1-like cluster was strongly, selectively and significantly
192 increased in the CSF as compared to the blood (Figure 2F, sFigure 5B). Conversely, the
193 CCR6$^+$GzmK$^+$ cluster was not enriched in the CSF, and CD4$^+$CTL (Cl 12) were even largely
194 excluded. TCR clonotype analysis unveiled further that only Tr1-like cells were clonally
195 expanded in the CSF of PwMS (Figure 2G). Conversely, no clonal expansions were detectable
196 in the CSF of control patients, with the caveat of the low cell numbers that are characteristic
197 for uninflamed CSF. Interestingly, in the blood of PwMS and in control patients only cytotoxic
198 clusters, i.e. CD4$^+$CTL, CCR6$^+$GzmK$^+$ and Tr1-like cells, contained expanded clones (sFigure 5C,
199 D). Moreover, we observed a significantly higher clonotype sharing between the Tr1 clusters
200 from the blood and the CSF in PwMS as compared to other clusters (Figure 2H), consistent
201 with an efficient recruitment of Tr1-cells from the blood to the CSF in PwMS.
202 Finally, to corroborate the enrichment of EOMES$^+$Tr1-like cells in the CSF, we analysed CD4$^+$T-
203 cell subsets also from the blood and the CSF in an independent cohort of treatment-naive RR-
204 PwMS (Table 1) by flow cytometry. EOMES$^+$Tr1-like cells were confirmed to be highly enriched
205 in the CSF (Figure 2I). Other subsets were not increased. Finally, all CD4$^+$T-cell subsets

206 expressed significantly higher levels of CXCR3 in the CSF as expected (Geginat et al., 2017;
207 Kendirli et al., 2023), and virtually all Tr1-like cells in the CSF were CXCR3$^+$ (sFigure 5E).
208 Collectively, these results show that EOMES$^+$Tr1-like cells can be identified in an unbiased
209 manner according to their unique gene expression profile and are strongly enriched and
210 clonally expanded in the CSF of PwMS.
211
212 **EOMES$^+$Tr1-like cells are the major IL-10 producing T-cell subset in the CSF of PwMS.**
213 Some *ex vivo* sequenced T-cells (Kendirli et al., 2023) expressed IL-10 mRNA. They belonged
214 mostly to the EOMES$^+$Tr1-like cluster (Figure 3A). Moreover, most IL-10$^+$ cells co-expressed
215 GzmK, but not FOXP3 and they were predominantly IL-7R^{lo} (sFigure 6A), suggesting that they
216 represent *in vivo* activated EOMES$^+$Tr1-like cells. Consistently, some IL-7R$^-$Tr1-like cells
217 expressed also IFN-γ. In contrast to IL-10$^+$T-cells, IFN-γ$^+$ and also IL-2$^+$ cells were however
218 present in several clusters and most co-expressed IL-7R (sFigure 6A).
219 We next analysed cytokine producing capacities of CD4$^+$T-cells in the CSF and in peripheral
220 blood of PwMS following brief stimulation with PMA and Ionomycin *ex vivo* by flow
221 cytometry. Unsupervised clustering identified ten T-cell clusters, including a single IL-10$^+$
222 cluster (Cl 9). The IL-10$^+$ cluster co-expressed EOMES, GzmK and IFN-γ and corresponded thus
223 to EOMES$^+$Tr1-like cells (sFigure 6B). In the CSF there was a strong enrichment for clusters
224 producing effector cytokines (Figure 3B, Cl 2-4 and 7-9). Cells in the effector cluster 8
225 contained pro-inflammatory EOMES$^+$GzmK$^+$cells ("inflam. GzmK$^+$") that expressed CD40L, IFN-
226 γ and GM-CSF (Codarri et al., 2011; Pulvirenti et al., 2024). In the blood most CD4$^+$T-cells
227 expressed instead exclusively CD40L (Figure 3B, Cl 1, "unpolarized"). We next investigated
228 possible differentiation pathways of the identified T-cell clusters by DiffusionMap analysis
229 (Figure 3C, sFigure 6C): Dimension 1 separated clusters according to effector cytokines into a
230 non-polarized and an effector group. Dimension 2 separated clusters furthermore according
231 to CD40L expression into helper and regulatory/effector cells. IL-10$^+$Tr1-like cells were
232 positioned on top of the pro-inflammatory GzmK$^+$ cluster, consistent with a precursor-
233 effector relationship (Geginat et al., 2023; Pulvirenti et al., 2024).
234 Notably, EOMES$^+$Tr1-like cells contained the highest percentages of IL-10$^+$ cells following brief
235 polyclonal stimulation of all CD4$^+$T-cell subsets in both HDs and in PwMS (Figure 3D). In
236 contrast to previous reports (Astier et al., 2006; Sumida et al., 2018), IL-10 producing
237 capacities of CD4$^+$T-cell subsets were not significantly reduced in the blood of PwMS, but they

238 were significantly increased in EOMES$^+$Tr1-like cells in the CSF. Notably, EOMES$^+$Tr1-like cells
239 could produce high amounts of IL-10 in the CSF of both RR- and P-PwMS (sFigure 6D). A
240 completely different pattern was as expected observed for IFN-γ (sFigure 6E). Thus, IFN-
241 γ producing capacities were in general very high in all cytotoxic subsets. Conversely, IFN-γ
242 producing capacities were low among Th-cells and Tregs in the blood, but they were strongly
243 increased in the CSF (Dominguez-Villar et al., 2011).
244 Although only a small fraction of Th-cells produced IL-10, they represent the large majority of
245 CD4$^+$T-cells and constituted consequently also the majority of IL-10 producing T-cells in the
246 blood (Figure 3E). Conversely, in the CSF of PwMS the major IL-10 producing T-cell subset
247 were EOMES$^+$Tr1-like cells, and also the contribution of Tregs was significantly increased.
248 In conclusion, regulatory T-cells -predominantly EOMES$^+$Tr1-like cells- could produce high
249 amounts of IL-10 in PwMS, in particular in the CSF.
250
251 **Regulatory T-cells in PwMS respond poorly to myelin antigens but are activated by EBV to**
252 **produce IFN-γ and IL-10.**
253 Antigenic activation induces T-cell proliferation and IL-10 production. We therefore
254 investigated if regulatory T-cells in MS patients reacted with a panel of self- and viral antigens
255 that we showed previously activate CSF-infiltrating CD4$^+$T-cells in PwMS (Paroni et al., 2017).
256 We modified an established assay to detect rare antigen-specific cells upon *ex vivo*
257 stimulation with antigenic peptides according to activation marker induction (Bacher et al.,
258 2013; Saggau et al., 2024), combining it with intracellular IL-10 and IFN-γ staining (sFigure 7).
259 The assay allows to monitor *ex vivo* frequencies and qualities of antigen-specific T-cells even
260 in a small amount of blood, which is often a limiting factor. Importantly, even rare antigen-
261 specific T-cells (<1:10.000) could be detected with high reproducibility (sFigure 7F).
262 Nevertheless, T-cell responses to the myelin-derived self-antigens MOG/MBP were hardly
263 detectable (Figure 4A, sFigure 7E). Only CD8$^+$T-cells and Th-cells showed statistically
264 significant responses in respectively untreated and Natalizumab-treated PwMS as compared
265 to the no peptide control (sFigure 8A). Importantly, EOMES$^+$Tr1-like cells largely failed to
266 respond at all to myelin antigens, including MOG, MBP and PLP (Figure 4A and sFigure 8A, B).
267 In contrast, we detected significant IFN-γ responses to EBV, i.e. to a commercially available
268 pool of immunodominant peptides, of EOMES$^+$Tr1-like cells in HD and PwMs (Figure 4A,

269 sFigure 8A). The response in HDs was low, but FACS-purified Tr1-like cells from HD
270 proliferated with EBV, maintaining GzmK and EOMES expression (Bonnal et al., 2021) (sFigure
271 7G), confirming thus that EOMES$^+$Tr1-like cells respond to EBV-derived antigens with a
272 different assay. Notably, however, proliferation-based assays underestimate antigen-specific
273 responses of anergic regulatory and exhausted/senescent effector T-cells (Geginat et al.,
274 2003; Haringer et al., 2009). Importantly, Th-cells and in particular EOMES$^+$Tr1-like cells
275 responded strongly to EBV in Natalizumab-treated PwMS. Conversely, CD4$^+$CTL and
276 CCR6$^+$GzmK$^+$ subsets responded poorly or not at all. Notably, CD8$^+$T-cells showed a strong
277 response to EBV in HDs that was further increased in PwMS, independently of Natalizumab
278 treatment (sFigure 8A). T-cell responses to JCV, a persistent virus that may cause progressive
279 multifocal leukoencephalopathy (PML) in Natalizumab-treated PwMS, showed a completely
280 different pattern. Thus, JCV activated predominantly Th-cells and CD4$^+$CTL, but only weakly
281 CD8$^+$T-cells and EOMES$^+$Tr1-like cells. Moreover, JCV-specific CD4$^+$T-cell responses were
282 overall reduced in treatment-naïve PwMS as compared to HDs and to Natalizumab-treated
283 PwMS (Figure 4A).
284 Interestingly, we detected also some IFN-γ production by FOXP3$^+$Tregs in response to EBV
285 (Figure 4A). Since only a minority of FOXP3$^+$Tregs can produce IFN-γ (sFigure 6E), we analysed
286 antigen-specific Treg responses also according to 4-1BB induction (Figure 4B), a well-
287 established read-out of TCR-induced Treg activation (Schoenbrunn et al., 2012). The antigen-
288 specific responses of FOXP3$^+$Treg were overall similar to EOMES$^+$Tr1-like cells. Thus, they
289 showed a weak EBV-specific response in HDs but responded strongly and significantly in
290 Natalizumab-treated PwMS. Responses of FOXP3$^+$Tregs to myelin-derived antigens and JCV
291 were in contrast low.
292 The strong increase of EBV-specific regulatory T-cells in Natalizumab-treated patients
293 suggested that they could migrate to the CNS. Consistently, we showed previously that CSF-
294 derived CCR6$^-$CXCR3$^+$"Th1"-cell lines of PwMS contained EBV-specific cells (Geginat et al.,
295 2017; Paroni et al., 2017). EOMES expression is stably maintained in CD4$^+$T-cell lines (sFigure
296 7G)(Bonnal et al., 2021), and here we found that a relevant fraction of CSF-derived "Th1"-cell
297 lines expressed EOMES (sFigure 8C), suggesting that they contained EOMES$^+$Tr1-like cells in
298 addition to conventional EOMES$^-$Th1-cells. These Eomes$^+$Tr1-like cells showed a robust IFN-γ
299 response to EBV-derived peptides (Figure 4C), suggesting that EOMES$^+$Tr1-like cells in the CSF

300 respond to EBV. Also EOMES$^-$Th1-cells responded as expected to EBV, but significantly
301 weaker.
302 EBV establishes a persistent, predominantly latent infection in B-cells, but can switch to lytic
303 infection that leads to the expression of several immunogenic proteins (Murata et al., 2021).
304 In Natalizumab-treated PwMS, EOMES$^+$Tr1-like cells were strongly activated by a peptide pool
305 of EBNA1 (Figure 4D, sFigure 9A), the most consistently expressed viral protein in latently
306 infected B-cells. Notably, in a patient that donated enough blood to sort EOMES$^+$Tr1-like cells,
307 we observed also a strong proliferative response to EBNA1 (sFigure 9B), confirming thus
308 EBNA1 specificity of Tr1-cells with an independent assay. In marked contrast, EOMES$^+$Tr1-like
309 cells responded poorly to two immunogenic lytic antigens (Figure 4D). Interestingly, Th-cells,
310 CD8$^+$T-cells and FOXP3$^+$Tregs responded in contrast also to lytic EBV antigens, in particular in
311 Natalizumab-treated patients (sFigure 9A).
312 We then investigated if EBV-specific T-cells could produce IL-10. Indeed, we were able to
313 detect significant IL-10 production by antigen-specific EOMES$^+$Tr1-like cells in response to the
314 immunodominant EBV peptide pool and to EBNA1, whereas IL-10 was undetectable with
315 myelin-derived peptides (Figure 4E). Similar results were obtained with FOXP3$^+$Tregs.
316 Conversely, antigen-specific IL-10 responses of Th-cells were variable and did not reach
317 statistical significance (sFigure 9C).
318 To understand if EBNA1-specific regulatory T-cells were a unique feature of MS, we finally
319 analyzed patients with systemic lupus erythematosus (SLE), a systemic autoimmune disease
320 that is also associated with EBV and may affect the CNS. Interestingly, EOMES$^+$Tr1-like cells
321 and FOXP3$^+$Tregs showed increased responses to EBV in SLE patients with CNS involvement
322 as compared to SLE patients without CNS involvement (Figure 4F, sFigure 10A, B).
323 Nevertheless, they failed to respond to EBNA1.
324 In conclusion, regulatory T-cells, particularly EOMES$^+$Tr1-like cells, are activated by the
325 latency-associated EBV-derived antigen EBNA1 in PwMS to produce IFN-γ and IL-10, but they
326 fail to respond to myelin-derived autoantigens.
327
328 **EBNA1-specific EOMES$^+$Tr1-like cells are associated with anti-EBNA1 IgG in PwMS and**
329 **disappear following therapeutic B-cell depletion.**
330 We next asked if EBV-specific regulatory T-cells cells were associated with the major genetic
331 risk factor of MS, the MHC class-II allele HLA-DRB1*15:01, which present antigenic peptides

332 to activate CD4$^+$T-cells (Tschochner et al., 2016). Individuals carrying this risk allele were
333 enriched among the analysed Natalizumab-treated PwMS (Table 3). IFN-γ responses of
334 EOMES$^+$Tr1-like cells in HLA-DRB1*15:01$^+$ PwMS to EBV-derived peptides were overall lower,
335 but they were clearly detectable and not significantly reduced (Figure 5A). EBV-specific IFN-γ
336 responses of Th -cells and Tregs were also similar, and also EBV-induced IL-10 production by
337 EOMES$^+$Tr1-like cells and FOXP3$^+$Tregs was not significantly altered (sFigure 11A).
338 Anti-EBNA1 IgG antibody levels represent a strong independent environmental risk factor of
339 MS (Bjornevik et al., 2023). Consistently, anti-EBNA1 IgG were significantly increased in both
340 untreated and Natalizumab-treated PwMS compared to HDs (sFigure 11B). EBNA1-specific,
341 IFN-γ-producing CD4$^+$T-cells were weakly associated (p-value: 0.0513) with anti-EBNA1 IgG
342 serum levels in Natalizumab-treated PwMS, and a weak tendency was also observed for
343 CD8$^+$T-cells (sFigure 11C). Intriguingly, a stronger and highly significant association was found
344 for EBNA1-specific EOMES$^+$Tr1-like cells (Figure 5B). Conversely, no association was found for
345 EBNA1-specific FOXP3$^+$Tregs (sFigure 11D). Moreover, there was also no association with
346 EBNA1-specific Th-cells, irrespectively if they were identified according to IFN-γ (Figure 5B) or
347 CD40L expression (sFigure 11E). Notably, EBNA1-activated EOMES$^+$ and FOPXP3$^+$ regulatory
348 T-cells largely failed in contrast to Th-cells to upregulate CD40L (Facciotti et al., 2016;
349 Schoenbrunn et al., 2012) (sFigure 11F), which is an absolute requirement for IgG induction
350 (Gordon, 1995).
351 We then asked if EBV-specific regulatory T-cells were affected by Ocrelizumab, a therapeutic
352 antibody depleting B-cells that could present EBV-derived peptides to T-cells. Ocrelizumab-
353 treated patients (Table 1) had strongly and significantly reduced CD8$^+$T-cell responses to EBV
354 (Abbadessa et al., 2024), consistent with ongoing T-cell activation by EBV antigen-presenting
355 B-cells in PwMS. Intriguingly, among CD4$^+$T-cells only EBV-specific EOMES$^+$Tr1-like cells were
356 significantly reduced, and they were in most cases undetectable (Figure 5C). Conversely, EBV-
357 specific FOXP3$^+$Tregs were not affected and EBV-specific Th-cells were only moderately
358 reduced.
359 Since both EOMES$^+$Tr1-cells and FOXP3$^+$T-cells could suppress CD8$^+$T-cell proliferation in
360 standard suppression assays (Bonnal et al., 2021; Pulvirenti et al., 2024), we investigated here
361 if they could also suppress CD8$^+$ memory T-cell activation induced by EBV-infected B-cells
362 (LCL, Figure 5D, sFigure 12). EOMES$^+$Tr1-like cells inhibited LCL-induced CD8$^+$T-cell

363 proliferation in a significant manner (Figure 5D). Surprisingly, FOXP3$^+$Tregs failed to suppress
364 and behaved overall similar to naïve CD4$^+$ control cells. Thus, they provided even help in some
365 experiments (Figure 5D, sFigure 12).
366 In conclusion, EBNA1-specific EOMES$^+$Tr1-like cells are present in PwMS expressing the HLA
367 risk allele, were associated with anti-EBNA1 IgG, disappeared following therapeutic B-cell
368 depletion and suppressed the activation of CD8$^+$ memory T-cells by EBV-infected B-cells.
369
370 **EOMES$^+$Tr1-like cells produce IL-10 in brain lesions of PwMS.**
371 Finally, to assess if EOMES$^+$Tr1-like cells were present in the CNS of PwMS, postmortem brain
372 sections of P-MS cases were stained for CD4, EOMES and IL-10 (Figure 6, sFigure 13).
373 EOMES$^+$IL-10$^+$CD4$^+$ cells were identified in three different MS cases. They were found in the
374 perivascular infiltrates of one active and one chronic active white matter lesion (Figure 6A, D-
375 F) and in the inflamed meninges (Fig. 6H and insets). Cells co-expressing CD4 and EOMES, but
376 not IL-10, were also detected (brown/red arrows in Figure 6A, H). They could represent either
377 pro-inflammatory cells (Raveney et al., 2021) or EOMES$^+$Tr1-like cells that were not activated
378 to produce IL-10 at the analysed time point. EOMES was as expected also detectable in CD4$^-$
379 cells (brown arrows in Figure 6A, H), and double staining of serial brain sections with anti-CD8
380 and anti-EOMES antibodies revealed the presence of EOMES$^+$CD8$^+$ cells in the same areas
381 (Figure 6, inset in I), suggesting a colocalization of EOMES$^+$Tr1-like cells and CD8$^+$
382 memory/effector T-cells in the brain of PwMS.
383 CD4$^+$ and CD4$^-$ cells expressing IL-10, but not EOMES, were also detectable (Figure 6, insets in
384 H), indicating that IL-10 production was not unique for EOMES$^+$Tr1-like cells. We therefore
385 counted cells in the brain sections to estimate the relative abundance of CNS-infiltrating
386 EOMES$^+$IL-10$^+$CD4$^+$Tr1-like cells. Approximately half of the IL-10$^+$ cells expressed CD4. CD4$^+$IL-
387 10$^+$EOMES$^+$Tr1-like cells represented 6,3±3% (mean ± SD) of total CD4$^+$T cells without any
388 appreciable difference between meningeal and parenchymal inflammatory cell infiltrates.
389 The percentages of CD4$^+$ cells expressing either EOMES or IL-10 alone were more variable
390 (EOMES$^+$: 14±10%; IL-10$^+$: 3.3±3.8%, respectively) and did again not differ significantly
391 between meningeal and parenchymal immune infiltrates. Thus, EOMES$^+$Tr1-like cells were a
392 major source of IL-10 among CD4$^+$T-cells also in these brain sections. Furthermore,
393 approximately one third of CD4$^+$EOMES$^+$T-cells stained positive for IL-10, i.e. a higher fraction
394 then those producing IL-10 upon stimulation with PMA and Ionomycin in the blood and the

395 CSF (Figure 3d). No IL-10 was in contrast detected in intraparenchymal neural cells and
396 microglia. Immunostaining for CD20 (Figure 6C, J), and *in situ* hybridization for the non-coding
397 EBV-derived RNA EBER (Figure 6G, K), performed in consecutive brain sections, revealed in
398 addition the presence of numerous EBV-infected B cells in the same immune infiltrates that
399 contained EOMES$^+$Tr1-like cells.
400 Overall, this analysis indicates that EOMES$^+$Tr1-like cells are present in the MS brain, some in
401 the vicinity of CD8$^+$T-cells or EBV-infected B-cells and are locally activated to produce IL-10.
402
403 **Discussion**
404 Eomes$^+$CD4$^+$T-cells contain both pro- and anti-inflammatory subsets, and have been proposed
405 to play a pathogenic role in EAE (Stienne et al., 2016) and in progressive MS (Raveney et al.,
406 2021). Our findings suggest a prominent role of anti-inflammatory EOMES$^+$Tr1-like cells in MS.
407 Thus, we documented here a dysregulated homeostasis selectively of EOMES$^+$Tr1-like cells in
408 MS that was related to their recruitment and activation in the CNS, where they were activated
409 to produce IL-10. We further showed that these adaptive regulatory T-cells could be activated
410 to produce IL-10 by the EBV antigen EBNA1, but not by myelin-derived antigens, suggesting
411 that they inhibit anti-EBV immune surveillance but are insufficient to prevent CNS
412 autoimmune pathology.
413 At variance with previous reports on defective IL-10 production by CD4$^+$T-cells in MS (Astier
414 et al., 2006; Sumida et al., 2018), and by our group in Inflammatory Bowel Diseases in the gut
415 (Alfen et al., 2018), we found that EOMES$^+$Tr1-like cells produced high amounts of IL-10 in the
416 CSF and in the brain of PwMS. Thus, a decrease of IL-10 producing T-cells in the blood of PwMS
417 is likely to reflect their recruitment to the CNS, but not a general defect of Tr1-cell
418 differentiation or IL-10 production. IL-10 exerts predominantly anti-inflammatory functions
419 in the CNS (Geginat et al., 2016). Nevertheless, also a role for T-cell derived IL-10 in sustaining
420 pathogenic T cell survival and CNS inflammation in EAE was recently proposed (Yogev et al.,
421 2022). In addition to IL-10, EOMES$^+$Tr1-like cells produce high levels of IFN-γ, but IFN-γ has a
422 neutral or even protective role in CNS inflammation (Dardalhon et al., 2008; Heinemann et
423 al., 2014). EOMES$^+$Tr1-like cells may however release cytotoxic molecules that could cause
424 collateral CNS damage (Haile et al., 2015; Terrabuio et al., 2025).

425 IL-10 production and proliferation of adaptive regulatory T-cells are controlled by T-cell
426 receptor stimulation. Therefore, the identification of the antigens that generate and activate
427 these cells is a key understudied issue to understand their functions, in particular in MS
428 (Paroni et al., 2017). In the EAE model, T-cells, including adaptive regulatory T-cells, are
429 deliberately primed by myelin-derived self-antigens. Conversely, in PwMS regulatory T-cells
430 largely failed to respond to three major CNS autoantigens. A failure to efficiently suppress
431 myelin-targeted autoimmunity could explain the extensive CNS damage in MS. An
432 unexpected key finding of this study is that regulatory T-cells in MS are activated by EBV, a
433 persistent virus that plays an essential detrimental role in MS (Bjornevik et al., 2022).
434 EOMES$^+$Tr1-like cells responded selectively to EBNA1, the viral protein that is most
435 consistently expressed in latently infected B-cells and therefore represents the virus' Achilles
436 heel (Murata et al., 2021). EBNA1 specific CD4$^+$T-cells in PwMS were previously reported to
437 represent Th1-cells (Lunemann et al., 2008), but since EOMES$^+$Tr1-cells were identified later,
438 these IFN-γ-producing CD4$^+$T-cells contained probably both conventional Th1-cells and
439 EOMES$^+$Tr1-like cells. We showed that EBNA1-specific EOMES$^+$Tr1-like cells were generated
440 in MS, but not in SLE patients with CNS involvement and are thus likely to represent a MS-
441 associated viral immune evasion strategy. Antibodies and T-cells that cross-react with EBNA1
442 and epitopes from self-proteins have been identified in PwMS (Geginat et al., 2017;
443 Lunemann et al., 2008; Tschochner et al., 2016; Wucherpfennig and Strominger, 1995),
444 suggesting that EBV infection might promote MS autoimmune pathology through molecular
445 mimicry. EOMES$^+$Tr1-like cells failed however to respond to myelin-derived antigens.
446 Consistently, a previous study showed that EBV-specific Th1 clones that failed to cross-react
447 with myelin antigens produced CCL4 rather than IL-2 (Lunemann et al., 2008), a pattern
448 reminiscent of Tr1-cells (Haringer et al., 2009). We can of course not exclude that EOMES$^+$Tr1-
449 like are activated by other cross-reactive antigens (Tschochner et al., 2016), but molecular
450 mimicry leading to the activation of regulatory T-cells in MS would be expected to have a
451 paradoxical beneficial effect.

452 EOMES$^+$Tr1-like cells lack B-cell helper functions and may suppress T-cell-dependent B-cell
453 responses unless they up-regulate CD40L (Facciotti et al., 2016). Since also EBNA1-specific
454 EOMES$^+$Tr1-like cells in MS failed to up-regulate CD40L, it seems highly unlikely that they
455 activate B-cells to produce anti-EBNA1 IgG antibodies. The association of EBNA1-specific IgG

456 and EOMES$^+$Tr1-like cells could rather reflect antigen presentation by EBNA1-specific B-cells,
457 which can internalize EBNA1 via their BCRs with very high efficiency to present EBNA1-derived
458 epitopes on MHC Class-II to CD4$^+$T-cells (Lanzavecchia, 1985). Consistently, EBNA1-specific
459 EOMES$^+$Tr1-like cells disappeared from the CD4$^+$T-cell compartment upon therapeutic B-cell
460 depletion in PwMS, suggesting that they are continuously generated by EBV antigen-
461 presenting B-cells. Anti-EBNA1 antibodies are produced by EBNA1-specific memory B-cells
462 following differentiation to plasma cells and may promote MS by molecular mimicry. EBNA1-
463 specific B-cells may in addition increase the risk of MS because they induce EBNA1-specific
464 regulatory T-cells that favor viral immune escape.

465 CD8$^+$T-cell responses to EBV are of broader magnitude in PwMS, and increased EBV
466 reactivation and CD8$^+$T-cell responses to lytic EBV antigens have been associated with active
467 disease (Angelini et al., 2013). Interestingly, CD8$^+$T-cells in PwMS recognise predominantly
468 lytic antigens (Schneider-Hohendorf et al., 2022), suggesting that immune surveillance of
469 latently infected B-cells may be inefficient. Intriguingly, immune-deficient mice reconstituted
470 with human immune cells from HLA-DRB1*15:01-positive individuals had an inefficient
471 control of EBV infection and mount dysregulated EBV-specific CD8$^+$T-cell responses
472 (Zdimerova et al., 2021), providing a link between the HLA risk haplotype and an inefficient
473 EBV immune control. EBNA1-specific Tr1-like cells were not significantly reduced in PwMS
474 carrying the HLA risk haplotype, indicating that EBNA1-derived epitopes that induce
475 EOMES$^+$Tr1-like cells are not necessarily HLA-DRB1*15:01-restricted. Finally, studies in post-
476 mortem brain tissue from PwMS suggested that EBV, which can be detected in B-cell enriched
477 inflammatory infiltrates in the CNS in a fraction of PwMS (Magliozzi et al., 2007), could lead
478 to the recruitment and activation of EBV-specific CD8$^+$T-cells (Magliozzi et al., 2007; Serafini
479 et al., 2019). Our finding that EOMES$^+$Tr1-like cells were present in the same CNS
480 inflammatory infiltrates where EBV$^+$B-cells and CD8$^+$T-cells were detectable supports the
481 concept that EOMES$^+$Tr1-like cells could inhibit EBV-specific immune responses in the CNS.
482 Indeed, EOMES$^+$Tr1-like cells, but not FOXP3$^+$Tregs, could suppress CD8$^+$T-cell responses
483 induced by EBV-infected B-cells *in vitro*. Thus, EBV-specific regulatory T-cells could inhibit
484 CD8$^+$T-cell-dependent immune surveillance of EBV (Geginat et al., 2017). This in turn could
485 promote the generation of EBNA1-specific EOMES$^+$Tr1-like cells due to persistent antigenic
486 stimulation in a positive feed-forward loop. EBV-specific regulatory T-cells may thus be both

487 a cause and a consequence of an inefficient anti-EBV immune control. CXCR3-dependent
488 migration of EBV-infected B-cells to the CNS (Laderach et al., 2025; Saraste et al., 2016) may
489 trigger the recruitment of virus-specific helper and regulatory T-cells (Angelini et al., 2013;
490 Balashov et al., 1999; Lossius et al., 2014; Magliozzi et al., 2013; Serafini et al., 2007; Serafini
491 et al., 2019; Serafini et al., 2010) and of auto-reactive Th1/17 bystander cells (Cao et al., 2015;
492 Paroni et al., 2017; Wang et al., 2020), leading ultimately to CNS damage (Geginat et al., 2017).
493 We thus propose that IL-10 produced by EBV-specific regulatory T-cells has a dual role in MS:
494 It could initially prevent collateral CNS damage in prodromal MS that develops after EBV
495 infections and is characterized by unsymptomatic CNS damage (Bjornevik et al., 2022).
496 However, since it favors viral immune escape, it enhances also the risk of EBV-associated
497 autoimmunity in the long run.

498 A lack of protection by regulatory T-cells is normally attributed to reduced Treg numbers or
499 functions, namely IL-10 production in MS. Our findings suggest the novel concept that Treg
500 dysfunction may also be a consequence of an aberrant antigen specificity, which promotes
501 immune evasion of a disease-promoting pathogen but is inefficient to inhibit auto-reactive T-
502 cells and immunopathology in the target tissue. A general implication of this study is further
503 that the analysis of polyclonal adaptive Treg populations without the knowledge of their
504 antigen specificities may be insufficient to understand their role in complex human
505 pathologies.

506

507 **Materials and Methods**

508

509 **Human samples**

510 Patient samples were collected at the MS Centre of the *Fondazione Ca' Granda, IRCCS*
511 *Ospedale Policlinico*, Milan ("Policlinico"), upon written informed consent, after Institutional
512 Ethical Committee approval (parere 708_2020). Patients were diagnosed according to the
513 revised McDonald criteria(Hartung et al., 2019). We collected 6-8 ml of peripheral blood
514 samples, by venous puncture, from 13 treatment-naïve patients affected by RR-MS (1-3d after
515 an attack), 4 untreated P-MS patients, 22 Natalizumab-treated RR-MS patients and 17
516 Ocrelizumab-treated MS patients (containing both RR and P-MS). For the latter, blood was
517 collected before the therapy session. 3-7 ml of CSF samples were obtained by lumbar

518 puncture from 7 untreated patients at diagnosis. In 5 of these patients also paired blood
519 samples were obtained. All patients whose CSF was analysed, were diagnosed as RR-MS and
520 had not received any previous treatment. Demographic and clinical characteristics of MS
521 patients and healthy donors (HD) enrolled in the study are shown in Table 1. As controls, 78
522 age- and sex-matched healthy donors were enrolled at the Policlinico upon informed consent.
523

524 **HLA genotyping**

525 Genomic DNA was isolated from peripheral blood using Qiagen columns. DNA was isolated
526 from frozen peripheral blood. DNA purification was performed with Qiagen EZ1 Advance XL
527 automated instrument using EZ1 DSP DNA Blood Kit (QIAGEN). HLA-DRB1 typing was
528 performed using Luminex based reverse SSO typing by using the LIFECODES HLA-DRB1 eRES
529 SSO Typing SSO typing kit (Immucor).
530

531 **Cell isolation and stimulation**

532 Peripheral blood mononuclear cells (PBMCs) were isolated from heparinized peripheral blood
533 by Ficoll-Hypaque gradient within 24h from blood withdrawal. Cells from CSF were collected
534 by centrifugation and analysed immediately. Plasma was collected and decomplemented or
535 stored at -80°C until use. PBMC were incubated for 4h at 37°C in a 5% CO2 humidified
536 atmosphere at a density of 2,5 x 10^6 cell/mL in RPMI complete medium (2 mM glutamine, 1
537 mM sodium pyruvate, 1% non-essential amino acids, 1% penicillin/streptomycin)
538 supplemented with 10% FCS in presence or absence of PMA (50 ng/mL) and Ionomycin (500
539 ng/mL). After 2h, Monensin (0.6 µl/ml,) was added and stimulated cells were stained for
540 superficial and intracellular markers (listed in sTable 4). For antigen -specific stimulations cells
541 were stimulated for 5 hours with peptide pools (EBV: Pool from 15 EBV proteins, or
542 overlapping peptide pools from EBNA1, BZLF1, BMRF1; JCV: VP1 plus VP2; Myelin: MOG, MBP,
543 PLP, Miltenyi) in medium without FCS that contained 5% autologous plasma. Incubation
544 without peptides was analysed as negative control, and with 100 ng/ml of the super-antigen
545 SEB as positive control. $CD4^+CXCR3^+CCR6^-$"Th1" and $CD4^+CCR6^+CXCR3^-$"Th17"-cells were
546 sorted from the CSF of untreated PwMS, excluding IL-$7R^{lo}CD25^+$Tregs. Cell lines were
547 generated as previously reported (Paroni et al., 2017) and restimulated with peptides as
548 described above.
549

550 **Flow Cytometry**

551 Cells were stained at the surface and intracellularly with fluorochrome-conjugated
552 monoclonal antibodies and live/dead (L/D) exclusion dye. The different panels of antibodies
553 (Ab) are represented in sTable 4. For surface staining, PBMCs were incubated for 20 min at
554 37°C, with the appropriate antibodies, including a L/D dye, diluted in Brilliant Staining Buffer
555 (BD). To stain for intracellular molecules samples were fixed with the
556 Fixation/Permeabilization working solution (eBioscience). For cytokine detection following
557 PMA plus Ionomycin stimulation cells were fixed with 2% PFA. Fixed cells were
558 permeabilized for 20 min at RT (eBioscience, Permeabilization Buffer). Cells were incubated
559 with the antibodies at 4°C for 120 minutes. Samples were acquired on a BD FACSymphony
560 and analysed with the BD FloJo Software. Antigen-specific $CD4^+$ and $CD8^+$T-cells were gated
561 as $CD69^+$IFN-γ^+ unless otherwise indicated. Antigen-stimulated $CD4^+$T-cell subsets cells were
562 in some cases also analysed for IL-10 production or CD40L up-regulation. Tregs were gated
563 as 4-$1BB^+CD69^+$ (Schoenbrunn et al., 2012). Notably, the markers used to identify T-cell
564 subsets (CD4, CD8, IL-7R, CCR6, FOXP3, GzmK, GzmB (Cossarizza et al., 2021)) were stably
565 expressed in the analysed time window (sFigure 4D).

566

567 **Suppression assay**

568 LCL lines were cultured standard complete RPMI medium. $CD8^+CD45RA^-$ memory T-cells were
569 sorted from PBMCs and stained with Cell Trace Violet Cell Proliferation Kit (INVITROGEN).
570 $CD4^+$T-cells were enriched using anti-CD4 magnetic microbeads (Miltenyi). Tr1 and Treg
571 subsets as well as $CD4^+CD45RA^+$ naïve control cells were then isolated by FACS sorting. LCL
572 and CD8 memory T-cells were seeded in 96 V shaped multiwell plates flasks in standard
573 complete RPMI (CORNING) in the absence or presence of $CD4^+$T-cell subsets and
574 Staphylococcus enterotoxin B (SEB, 1 µg/mL) added. The ratio between LCL, $CD8^+$ and $CD4^+$
575 T-cells was 0.5:1:1 After 7 days of co-culture cells were collected and Cell Trace Dilution of
576 CD8+ T-cells assessed. Analysis of FCS data was performed using BD FlowJo software
577 (proliferation modeling tool).

578

579 **Anti-EBNA1 ELISA**

580 ELISA to measure the levels of anti-EBNA1 IgG were performed using serum diluted 1:5 with
581 a kit (Serion Diagnostics) following the manufacturer's instructions.

582

583 **scRNAseq data**

584 Processed single-cell RNA sequencing (scRNA-seq) gene expression data were obtained from
585 the Gene Expression Omnibus (GEO) database under the accession number GSE232343
586 (Kendirli et al., 2023). The data were subsequently analyzed using the Seurat package (v.5.0.1)
587 in R. The scRNA-seq dataset contained clusters defined in the original study. We utilized
588 Seurat's FindMarkers function with default parameters and Wilcoxon test to obtain
589 Differentially Expressed Genes (DEGs) for each cluster. Clusters were labelled using the DEGs
590 and additional information of known $CD4^+$T-cell subset markers. To identify DEGs between
591 conditions within the same $CD4^+$T-cell subpopulation, we employed a pseudobulk approach.
592 This method aggregates single-cell counts within each condition/patient to create bulk-like
593 profiles, thereby improving the robustness of the differential expression analysis. Gene set
594 enrichment analysis (GSEA) was performed using the fgsea() function from the fgsea package
595 (v1.20.0). The reference Tr1 associated gene set for the analysis was obtained from our
596 previous studies(Bonnal et al., 2021; De Simone et al., 2021). For TCR analysis, we selected
597 cells with paired alpha and beta chain sequenced (69112 cells). TCR overlap was defined as
598 the presence of identical paired alpha-beta chains in cells of the same cell-type across the two
599 tissues. Clonal diversity within each cluster was assessed using the normalized Shannon's
600 diversity index. For a given cluster with S unique clonotypes and relative frequencies p_i, the
601 Shannon index was calculated as $H' = -\sum_{i=1}^{S} p_i \ln(p_i)$. To account for differences in cluster
602 size, was normalized by the maximum possible value $\ln(S)$. To better capture clonal
603 expansion, we used the inverted form of the index: $H'_{inv} = 1 - \frac{H'}{\ln(S)}$, where higher values
604 reflect reduced diversity and dominance by fewer clonotypes.

605

606 **Statistical analysis**

607 Data were analysed with FlowJo software (Tree Star Inc, v. 10.8), while the statistical analyses
608 were performed with Prism10 software (GraphPad). Student t-test were performed to
609 compare two groups, a paired t-test for values derived from the same individuals, and an
610 unpaired t-test to compare two different cohorts. One-way ANOVA was used to compare a
611 single parameter in multiple groups, two-way ANOVA to compare multiple values in multiple
612 groups. P-values <0.05 (*), <0.01 (**), < 0.001 (***), < 0.0001 (****) were regarded as

statistically significant. Where indicated, borderline p-values (0.05-0.1) were reported in the panels.

615 **Tissue samples and immunostainings**

616 Sections from 5 well-characterized post-mortem brain tissue blocks from 4 donors with
617 progressive MS, provided by the UK Multiple Sclerosis Tissue Bank at Imperial College London
618 (https://www.imperial.ac.uk/medicine/multiple-sclerosis-and-parkinsons-tissue-bank/) were
619 analysed. The use of human tissue for research purposes was approved by the Ethics
620 Committee of Istituto Superiore di Sanità (2023_0059846). Tissue sections used in this study
621 contained substantial immune infiltrates with CD4+ and CD8+ T cells in the white matter
622 (WM) and meninges. Triple immunostainings in bright field were performed with mouse anti-
623 EOMES, rat anti-IL-10 and rabbit anti-CD4 purified monoclonal antibodies (see supplementary
624 Methods). Negative control stainings were performed in consecutive sections using rat and
625 mouse Ig isotype controls (ThermoFisher, sFigure 13). In serial sections immunostainigs for
626 CD8, CD20 and EBER (Serafini et al., 2023) and double stainings with rabbit polyclonal anti-
627 CD8 (Thermo Fisher Scientific) and anti-EOMES were also performed. Stained sections were
628 analysed and images acquired with an Axioscope microscope (Carl Zeiss, Jena, Germany)
629 equipped with AxioCam MRc5 camera and Axiovision SE 64 software. Cell counts were
630 performed manually in the immune infiltrates containing $CD4^+$ cells on the entire sections,
631 both the WM and meninges, with a morphometric grid within the ocular lens, at 20x
632 magnification. Data are expressed as mean $\pm$SD values of the percentages of triple positive
633 $EOMES^+IL10^+CD4^+$ cells in the total $CD4^+$T-cell population.

634

635 **Acknowledgments**

636 This work was supported by FISM - Fondazione Italiana Sclerosi Multipla (2017/R/14) and co-
637 financed with the '5 per mille' public funding. This project has received also funding from the
638 European Union's Horizon Europe Research and Innovation Actions under grant no.
639 101137235 (BEHIND-MS). Views and opinions expressed are however those of the author(s)
640 only and do not necessarily reflect those of the European Union nor the granting authority.
641 Neither the European Union nor the granting authority can be held responsible for them. DG
642 and ES are supported by the Italian Ministry of Health (Ricerca Corrente). We thank Manuel
643 Albanese and Samuele Nortabartolo for critical reading and comments, and Francesca Aloisi
644 for inspiring discussion and suggestions.

645

Conflict of interest

The authors have no conflicts of interest to declare.

650 **References**

651 Abbadessa, G., Lepore, M.T., Bruzzaniti, S., Piemonte, E., Miele, G., Signoriello, E., Perna, F.,
652 De Falco, C., Lus, G., Matarese, G.*, et al.* (2024). Ocrelizumab Alters Cytotoxic Lymphocyte
653 Function While Reducing EBV-Specific CD8(+) T-Cell Proliferation in Patients With Multiple
654 Sclerosis. Neurol Neuroimmunol Neuroinflamm *11*, e200250.
655 Alfen, J.S., Larghi, P., Facciotti, F., Gagliani, N., Bosotti, R., Paroni, M., Maglie, S., Gruarin, P.,
656 Vasco, C.M., Ranzani, V.*, et al.* (2018). Intestinal IFN-gamma-producing Tr1-cells co-express
657 CCR5 and PD-1, and down-regulate IL-10 in the inflamed guts of IBD patients. J Allergy Clin
658 Immunol.
659 Aloisi, F., Giovannoni, G., and Salvetti, M. (2023). Epstein-Barr virus as a cause of multiple
660 sclerosis: opportunities for prevention and therapy. Lancet Neurol *22*, 338-349.
661 Anderson, C.F., Oukka, M., Kuchroo, V.J., and Sacks, D. (2007). CD4(+)CD25(-)Foxp3(-) Th1
662 cells are the source of IL-10-mediated immune suppression in chronic cutaneous
663 leishmaniasis. J Exp Med *204*, 285-297.
664 Angelini, D.F., Serafini, B., Piras, E., Severa, M., Coccia, E.M., Rosicarelli, B., Ruggieri, S.,
665 Gasperini, C., Buttari, F., Centonze, D.*, et al.* (2013). Increased CD8+ T cell response to Epstein-
666 Barr virus lytic antigens in the active phase of multiple sclerosis. PLoS Pathog *9*, e1003220.
667 Astier, A.L., Meiffren, G., Freeman, S., and Hafler, D.A. (2006). Alterations in CD46-mediated
668 Tr1 regulatory T cells in patients with multiple sclerosis. The Journal of clinical investigation
669 *116*, 3252-3257.
670 Bacher, P., Schink, C., Teutschbein, J., Kniemeyer, O., Assenmacher, M., Brakhage, A.A., and
671 Scheffold, A. (2013). Antigen-reactive T cell enrichment for direct, high-resolution analysis of
672 the human naive and memory Th cell repertoire. J Immunol *190*, 3967-3976.
673 Balashov, K.E., Rottman, J.B., Weiner, H.L., and Hancock, W.W. (1999). CCR5(+) and CXCR3(+)
674 T cells are increased in multiple sclerosis and their ligands MIP-1alpha and IP-10 are expressed
675 in demyelinating brain lesions. Proc. Natl. Acad. Sci. U. S. A. *96*, 6873-6878.
676 Bjornevik, K., Cortese, M., Healy, B.C., Kuhle, J., Mina, M.J., Leng, Y., Elledge, S.J., Niebuhr,
677 D.W., Scher, A.I., Munger, K.L., and Ascherio, A. (2022). Longitudinal analysis reveals high
678 prevalence of Epstein-Barr virus associated with multiple sclerosis. Science *375*, 296-301.
679 Bjornevik, K., Munz, C., Cohen, J.I., and Ascherio, A. (2023). Epstein-Barr virus as a leading
680 cause of multiple sclerosis: mechanisms and implications. Nat Rev Neurol *19*, 160-171.
681 Bonnal, R.J.P., Rossetti, G., Lugli, E., De Simone, M., Gruarin, P., Brummelman, J., Drufuca, L.,
682 Passaro, M., Bason, R., Gervasoni, F.*, et al.* (2021). Clonally expanded EOMES(+) Tr1-like cells
683 in primary and metastatic tumors are associated with disease progression. Nat Immunol *22*,
684 735-745.
685 Brockmann, L., Soukou, S., Steglich, B., Czarnewski, P., Zhao, L., Wende, S., Bedke, T., Ergen,
686 C., Manthey, C., Agalioti, T.*, et al.* (2018). Molecular and functional heterogeneity of IL-10-
687 producing CD4(+) T cells. Nat Commun *9*, 5457.
688 Buckner, J.H. (2010). Mechanisms of impaired regulation by CD4(+)CD25(+)FOXP3(+)
689 regulatory T cells in human autoimmune diseases. Nat Rev Immunol *10*, 849-859.
690 Cao, Y., Goods, B.A., Raddassi, K., Nepom, G.T., Kwok, W.W., Love, J.C., and Hafler, D.A. (2015).
691 Functional inflammatory profiles distinguish myelin-reactive T cells from patients with
692 multiple sclerosis. Sci Transl Med *7*, 287ra274.
693 Carbone, F., De Rosa, V., Carrieri, P.B., Montella, S., Bruzzese, D., Porcellini, A., Procaccini, C.,
694 La Cava, A., and Matarese, G. (2014). Regulatory T cell proliferative potential is impaired in
695 human autoimmune disease. Nat Med *20*, 69-74.
696 Christensen, T. (2006). The role of EBV in MS pathogenesis. Int MS J *13*, 52-57.

697 Codarri, L., Gyulveszi, G., Tosevski, V., Hesske, L., Fontana, A., Magnenat, L., Suter, T., and
698 Becher, B. (2011). RORgammat drives production of the cytokine GM-CSF in helper T cells,
699 which is essential for the effector phase of autoimmune neuroinflammation. Nature
700 immunology *12*, 560-567.
701 Cossarizza, A., Chang, H.D., Radbruch, A., Abrignani, S., Addo, R., Akdis, M., Andra, I.,
702 Andreata, F., Annunziato, F., Arranz, E.*, et al.* (2021). Guidelines for the use of flow cytometry
703 and cell sorting in immunological studies (third edition). Eur J Immunol *51*, 2708-3145.
704 Dardalhon, V., Korn, T., Kuchroo, V.K., and Anderson, A.C. (2008). Role of Th1 and Th17 cells
705 in organ-specific autoimmunity. J Autoimmun *31*, 252-256.
706 De Simone, M., Chirichella, M., Emming, S., Mazzara, S., Ranzani, V., Gruarin, P., Moschetti,
707 G., Pulvirenti, N., Maglie, S., Vasco, C.*, et al.* (2021). Ex vivo microRNA and gene expression
708 profiling of human Tr1-like cells suggests a role for miR-92a and -125a in the regulation of
709 EOMES and IL-10R. Eur J Immunol.
710 Dejean, A.S., Joulia, E., and Walzer, T. (2019). The role of Eomes in human CD4 T cell
711 differentiation: A question of context. Eur J Immunol *49*, 38-41.
712 Dominguez-Villar, M., Baecher-Allan, C.M., and Hafler, D.A. (2011). Identification of T helper
713 type 1-like, Foxp3+ regulatory T cells in human autoimmune disease. Nat Med *17*, 673-675.
714 Facciotti, F., Gagliani, N., Haringer, B., Alfen, J.S., Penatti, A., Maglie, S., Paroni, M., Iseppon,
715 A., Moro, M., Crosti, M.C.*, et al.* (2016). IL-10-producing forkhead box protein 3-negative
716 regulatory T cells inhibit B-cell responses and are involved in systemic lupus erythematosus. J
717 Allergy Clin Immunol *137*, 318-321 e315.
718 Gabrysova, L., Nicolson, K.S., Streeter, H.B., Verhagen, J., Sabatos-Peyton, C.A., Morgan, D.J.,
719 and Wraith, D.C. (2009). Negative feedback control of the autoimmune response through
720 antigen-induced differentiation of IL-10-secreting Th1 cells. J Exp Med *206*, 1755-1767.
721 Gagliani, N., Jofra, T., Stabilini, A., Valle, A., Atkinson, M., Roncarolo, M.G., and Battaglia, M.
722 (2010). Antigen-specific dependence of Tr1-cell therapy in preclinical models of islet
723 transplant. Diabetes *59*, 433-439.
724 Geginat, J., Lanzavecchia, A., and Sallusto, F. (2003). Proliferation and differentiation potential
725 of human CD8+ memory T-cell subsets in response to antigen or homeostatic cytokines. Blood
726 *101*, 4260-4266.
727 Geginat, J., Larghi, P., Paroni, M., Nizzoli, G., Penatti, A., Pagani, M., Gagliani, N., Meroni, P.,
728 Abrignani, S., and Flavell, R.A. (2016). The light and the dark sides of Interleukin-10 in immune-
729 mediated diseases and cancer. Cytokine & growth factor reviews.
730 Geginat, J., Paroni, M., Pagani, M., Galimberti, D., De Francesco, R., Scarpini, E., and Abrignani,
731 S. (2017). The Enigmatic Role of Viruses in Multiple Sclerosis: Molecular Mimicry or Disturbed
732 Immune Surveillance? Trends Immunol.
733 Geginat, J., Vasco, C., Gruarin, P., Bonnal, R., Rossetti, G., Silvestri, Y., Carelli, E., Pulvirenti, N.,
734 Scantamburlo, M., Moschetti, G.*, et al.* (2023). Eomesodermin-expressing type 1 regulatory
735 (EOMES(+) Tr1)-like T cells: Basic biology and role in immune-mediated diseases. Eur J
736 Immunol, e2149775.
737 Gordon, J. (1995). CD40 and its ligand: central players in B lymphocyte survival, growth, and
738 differentiation. Blood Rev *9*, 53-56.
739 Gruarin, P., Maglie, S., De Simone, M., Haringer, B., Vasco, C., Ranzani, V., Bosotti, R.,
740 Noddings, J.S., Larghi, P., Facciotti, F.*, et al.* (2019). Eomesodermin controls a unique
741 differentiation program in human IL-10 and IFN-gamma coproducing regulatory T cells. Eur J
742 Immunol *49*, 96-111.

743 Haile, Y., Carmine-Simmen, K., Olechowski, C., Kerr, B., Bleackley, R.C., and Giuliani, F. (2015).
744 Granzyme B-inhibitor serpina3n induces neuroprotection in vitro and in vivo. J
745 Neuroinflammation *12*, 157.
746 Haringer, B., Lozza, L., Steckel, B., and Geginat, J. (2009). Identification and characterization
747 of IL-10/IFN-gamma-producing effector-like T cells with regulatory function in human blood.
748 J Exp Med *206*, 1009-1017.
749 Hartung, H.P., Graf, J., Aktas, O., Mares, J., and Barnett, M.H. (2019). Diagnosis of multiple
750 sclerosis: revisions of the McDonald criteria 2017 - continuity and change. Curr Opin Neurol
751 *32*, 327-337.
752 Heinemann, C., Heink, S., Petermann, F., Vasanthakumar, A., Rothhammer, V., Doorduijn, E.,
753 Mitsdoerffer, M., Sie, C., Prazeres da Costa, O., Buch, T.*, et al.* (2014). IL-27 and IL-12 oppose
754 pro-inflammatory IL-23 in CD4+ T cells by inducing Blimp1. Nat Commun *5*, 3770.
755 Hrastelj, J., Andrews, R., Loveless, S., Morgan, J., Bishop, S.M., Bray, N.J., Williams, N.M., and
756 Robertson, N.P. (2021). CSF-resident CD4(+) T-cells display a distinct gene expression profile
757 with relevance to immune surveillance and multiple sclerosis. Brain Commun *3*, fcab155.
758 Jankovic, D., Kullberg, M.C., Feng, C.G., Goldszmid, R.S., Collazo, C.M., Wilson, M., Wynn, T.A.,
759 Kamanaka, M., Flavell, R.A., and Sher, A. (2007). Conventional T-bet(+)Foxp3(-) Th1 cells are
760 the major source of host-protective regulatory IL-10 during intracellular protozoan infection.
761 J Exp Med *204*, 273-283.
762 Jeon, S.G., Kayama, H., Ueda, Y., Takahashi, T., Asahara, T., Tsuji, H., Tsuji, N.M., Kiyono, H.,
763 Ma, J.S., Kusu, T.*, et al.* (2012). Probiotic Bifidobacterium breve induces IL-10-producing Tr1
764 cells in the colon. PLoS pathogens *8*, e1002714.
765 Kendirli, A., de la Rosa, C., Lammle, K.F., Eglseer, K., Bauer, I.J., Kavaka, V., Winklmeier, S.,
766 Zhuo, L., Wichmann, C., Gerdes, L.A.*, et al.* (2023). A genome-wide in vivo CRISPR screen
767 identifies essential regulators of T cell migration to the CNS in a multiple sclerosis model. Nat
768 Neurosci *26*, 1713-1725.
769 Kivisakk, P., Healy, B.C., Viglietta, V., Quintana, F.J., Hootstein, M.A., Weiner, H.L., and Khoury,
770 S.J. (2009). Natalizumab treatment is associated with peripheral sequestration of
771 proinflammatory T cells. Neurology *72*, 1922-1930.
772 Kuchroo, V.K., and Weiner, H.L. (2022). How does Epstein-Barr virus trigger MS? Immunity *55*,
773 390-392.
774 Laderach, F., Piteros, I., Fennell, E., Bremer, E., Last, M., Schmid, S., Rieble, L., Campbell, C.,
775 Ludwig-Portugall, I., Bornemann, L.*, et al.* (2025). EBV induces CNS homing of B cells attracting
776 inflammatory T cells. Nature *646*, 171-179.
777 Lanzavecchia, A. (1985). Antigen-specific interaction between T and B cells. Nature *314*, 537-
778 539.
779 Lossius, A., Johansen, J.N., Vartdal, F., Robins, H., Jurate Saltyte, B., Holmoy, T., and Olweus,
780 J. (2014). High-throughput sequencing of TCR repertoires in multiple sclerosis reveals
781 intrathecal enrichment of EBV-reactive CD8+ T cells. Eur J Immunol *44*, 3439-3452.
782 Lunemann, J.D., Jelcic, I., Roberts, S., Lutterotti, A., Tackenberg, B., Martin, R., and Munz, C.
783 (2008). EBNA1-specific T cells from patients with multiple sclerosis cross react with myelin
784 antigens and co-produce IFN-gamma and IL-2. The Journal of experimental medicine *205*,
785 1763-1773.
786 Magliozzi, R., Howell, O., Vora, A., Serafini, B., Nicholas, R., Puopolo, M., Reynolds, R., and
787 Aloisi, F. (2007). Meningeal B-cell follicles in secondary progressive multiple sclerosis
788 associate with early onset of disease and severe cortical pathology. Brain *130*, 1089-1104.

789 Magliozzi, R., Serafini, B., Rosicarelli, B., Chiappetta, G., Veroni, C., Reynolds, R., and Aloisi, F.
790 (2013). B-cell enrichment and Epstein-Barr virus infection in inflammatory cortical lesions in
791 secondary progressive multiple sclerosis. J Neuropathol Exp Neurol *72*, 29-41.
792 Mazzoni, A., Maggi, L., Siracusa, F., Ramazzotti, M., Rossi, M.C., Santarlasci, V., Montaini, G.,
793 Capone, M., Rossettini, B., De Palma, R.*, et al.* (2018). Eomes controls the development of
794 Th17-derived (non-classic) Th1 cells during chronic inflammation. Eur J Immunol.
795 Murata, T., Sugimoto, A., Inagaki, T., Yanagi, Y., Watanabe, T., Sato, Y., and Kimura, H. (2021).
796 Molecular Basis of Epstein-Barr Virus Latency Establishment and Lytic Reactivation. Viruses
797 *13*.
798 Noori-Zadeh, A., Mesbah-Namin, S.A., Bistoon-Beigloo, S., Bakhtiyari, S., Abbaszadeh, H.A.,
799 Darabi, S., Rajabibazl, M., and Abdanipour, A. (2016). Regulatory T cell number in multiple
800 sclerosis patients: A meta-analysis. Mult Scler Relat Disord *5*, 73-76.
801 O'Garra, A., and Vieira, P. (2007). T(H)1 cells control themselves by producing interleukin-10.
802 Nat Rev Immunol *7*, 425-428.
803 Ochs, H.D., Gambineri, E., and Torgerson, T.R. (2007). IPEX, FOXP3 and regulatory T-cells: a
804 model for autoimmunity. Immunologic research *38*, 112-121.
805 Olsson, T., Barcellos, L.F., and Alfredsson, L. (2017). Interactions between genetic, lifestyle
806 and environmental risk factors for multiple sclerosis. Nat Rev Neurol *13*, 25-36.
807 Parish, I.A., Marshall, H.D., Staron, M.M., Lang, P.A., Brustle, A., Chen, J.H., Cui, W., Tsui, Y.C.,
808 Perry, C., Laidlaw, B.J.*, et al.* (2014). Chronic viral infection promotes sustained Th1-derived
809 immunoregulatory IL-10 via BLIMP-1. The Journal of clinical investigation.
810 Paroni, M., Maltese, V., De Simone, M., Ranzani, V., Larghi, P., Fenoglio, C., Pietroboni, A.M.,
811 De Riz, M.A., Crosti, M.C., Maglie, S.*, et al.* (2017). Recognition of viral and self-antigens by
812 TH1 and TH1/TH17 central memory cells in patients with multiple sclerosis reveals distinct
813 roles in immune surveillance and relapses. J Allergy Clin Immunol.
814 Peeters, L.M., Vanheusden, M., Somers, V., Van Wijmeersch, B., Stinissen, P., Broux, B., and
815 Hellings, N. (2017). Cytotoxic CD4+ T Cells Drive Multiple Sclerosis Progression. Front Immunol
816 *8*, 1160.
817 Pulvirenti, N., Silvetri, Y., Clemente, F., Bosotti, R., Carelli, E., Moschetti, G., Gruarin, P., Vasco,
818 C., Crosti, M.C., Sarnicola, M.L.*, et al.* (2024). Characterization of human CD4(+) EOMES(+)
819 GzmK(+) T-cell subsets unveils an uncoupling of suppressive functions from IL-10-producing
820 capacities. Eur J Immunol, e2350675.
821 Raveney, B.J.E., Sato, W., Takewaki, D., Zhang, C., Kanazawa, T., Lin, Y., Okamoto, T., Araki,
822 M., Kimura, Y., Sato, N.*, et al.* (2021). Involvement of cytotoxic Eomes-expressing CD4(+) T
823 cells in secondary progressive multiple sclerosis. Proc Natl Acad Sci U S A *118*.
824 Roncarolo, M.G., Gregori, S., Battaglia, M., Bacchetta, R., Fleischhauer, K., and Levings, M.K.
825 (2006). Interleukin-10-secreting type 1 regulatory T cells in rodents and humans.
826 Immunological reviews *212*, 28-50.
827 Saggau, C., Bacher, P., Esser, D., Rasa, M., Meise, S., Mohr, N., Kohlstedt, N., Hutloff, A.,
828 Schacht, S.S., Dargvainiene, J.*, et al.* (2024). Autoantigen-specific CD4(+) T cells acquire an
829 exhausted phenotype and persist in human antigen-specific autoimmune diseases. Immunity
830 *57*, 2416-2432 e2418.
831 Sakaguchi, S., Ono, M., Setoguchi, R., Yagi, H., Hori, S., Fehervari, Z., Shimizu, J., Takahashi, T.,
832 and Nomura, T. (2006). Foxp3+ CD25+ CD4+ natural regulatory T cells in dominant self-
833 tolerance and autoimmune disease. Immunological reviews *212*, 8-27.
834 Saraste, M., Penttila, T.L., and Airas, L. (2016). Natalizumab treatment leads to an increase in
835 circulating CXCR3-expressing B cells. Neurol Neuroimmunol Neuroinflamm *3*, e292.

836 Schneider-Hohendorf, T., Gerdes, L.A., Pignolet, B., Gittelman, R., Ostkamp, P., Rubelt, F.,
837 Raposo, C., Tackenberg, B., Riepenhausen, M., Janoschka, C.*, et al.* (2022). Broader Epstein-
838 Barr virus-specific T cell receptor repertoire in patients with multiple sclerosis. J Exp Med *219*.
839 Schoenbrunn, A., Frentsch, M., Kohler, S., Keye, J., Dooms, H., Moewes, B., Dong, J.,
840 Loddenkemper, C., Sieper, J., Wu, P.*, et al.* (2012). A converse 4-1BB and CD40 ligand
841 expression pattern delineates activated regulatory T cells (Treg) and conventional T cells
842 enabling direct isolation of alloantigen-reactive natural Foxp3+ Treg. Journal of immunology
843 *189*, 5985-5994.
844 Serafini, B., Rosicarelli, B., Franciotta, D., Magliozzi, R., Reynolds, R., Cinque, P., Andreoni, L.,
845 Trivedi, P., Salvetti, M., Faggioni, A., and Aloisi, F. (2007). Dysregulated Epstein-Barr virus
846 infection in the multiple sclerosis brain. J Exp Med *204*, 2899-2912.
847 Serafini, B., Rosicarelli, B., Veroni, C., and Aloisi, F. (2023). Tissue-resident memory T cells in
848 the multiple sclerosis brain and their relationship to Epstein-Barr virus infected B cells. J
849 Neuroimmunol *376*, 578036.
850 Serafini, B., Rosicarelli, B., Veroni, C., Mazzola, G.A., and Aloisi, F. (2019). Epstein-Barr Virus-
851 Specific CD8 T Cells Selectively Infiltrate the Brain in Multiple Sclerosis and Interact Locally
852 with Virus-Infected Cells: Clue for a Virus-Driven Immunopathological Mechanism. J Virol *93*.
853 Serafini, B., Severa, M., Columba-Cabezas, S., Rosicarelli, B., Veroni, C., Chiappetta, G.,
854 Magliozzi, R., Reynolds, R., Coccia, E.M., and Aloisi, F. (2010). Epstein-Barr virus latent
855 infection and BAFF expression in B cells in the multiple sclerosis brain: implications for viral
856 persistence and intrathecal B-cell activation. J Neuropathol Exp Neurol *69*, 677-693.
857 Stienne, C., Michieletto, M.F., Benamar, M., Carrie, N., Bernard, I., Nguyen, X.H., Lippi, Y.,
858 Duguet, F., Liblau, R.S., Hedrick, S.M.*, et al.* (2016). Foxo3 Transcription Factor Drives
859 Pathogenic T Helper 1 Differentiation by Inducing the Expression of Eomes. Immunity *45*, 774-
860 787.
861 Suffia, I.J., Reckling, S.K., Piccirillo, C.A., Goldszmid, R.S., and Belkaid, Y. (2006). Infected site-
862 restricted Foxp3+ natural regulatory T cells are specific for microbial antigens. J Exp Med *203*,
863 777-788.
864 Sumida, T., Lincoln, M.R., Ukeje, C.M., Rodriguez, D.M., Akazawa, H., Noda, T., Naito, A.T.,
865 Komuro, I., Dominguez-Villar, M., and Hafler, D.A. (2018). Activated beta-catenin in Foxp3(+)
866 regulatory T cells links inflammatory environments to autoimmunity. Nat Immunol *19*, 1391-
867 1402.
868 Terrabuio, E., Pietronigro, E.C., Bani, A., Della Bianca, V., Laudanna, C., Rossi, B., Finotti, G.,
869 Santos-Lima, B., Zenaro, E., Turano, E.*, et al.* (2025). CD103(-)CD8(+) T cells promote
870 neurotoxic inflammation in Alzheimer's disease via granzyme K-PAR-1 signaling. Nat Commun
871 *16*, 8372.
872 Thelen, B., Schipperges, V., Knorlein, P., Hummel, J.F., Arnold, F., Kupferschmid, L., Klose,
873 C.S.N., Arnold, S.J., Boerries, M., and Tanriver, Y. (2023). Eomes is sufficient to regulate IL-10
874 expression and cytotoxic effector molecules in murine CD4(+) T cells. Front Immunol *14*,
875 1058267.
876 Tschochner, M., Leary, S., Cooper, D., Strautins, K., Chopra, A., Clark, H., Choo, L., Dunn, D.,
877 James, I., Carroll, W.M.*, et al.* (2016). Identifying Patient-Specific Epstein-Barr Nuclear
878 Antigen-1 Genetic Variation and Potential Autoreactive Targets Relevant to Multiple Sclerosis
879 Pathogenesis. PLoS One *11*, e0147567.
880 Wang, J., Jelcic, I., Muhlenbruch, L., Haunerdinger, V., Toussaint, N.C., Zhao, Y., Cruciani, C.,
881 Faigle, W., Naghavian, R., Foege, M.*, et al.* (2020). HLA-DR15 Molecules Jointly Shape an
882 Autoreactive T Cell Repertoire in Multiple Sclerosis. Cell *183*, 1264-1281 e1220.

883 Wucherpfennig, K.W., and Strominger, J.L. (1995). Molecular mimicry in T cell-mediated
884 autoimmunity: viral peptides activate human T cell clones specific for myelin basic protein.
885 Cell *80*, 695-705.
886 Yogev, N., Bedke, T., Kobayashi, Y., Brockmann, L., Lukas, D., Regen, T., Croxford, A.L., Nikolav,
887 A., Hovelmeyer, N., von Stebut, E.*, et al.* (2022). CD4(+) T-cell-derived IL-10 promotes CNS
888 inflammation in mice by sustaining effector T cell survival. Cell Rep *38*, 110565.
889 Zdimerova, H., Murer, A., Engelmann, C., Raykova, A., Deng, Y., Gujer, C., Ruhl, J., McHugh,
890 D., Caduff, N., Naghavian, R.*, et al.* (2021). Attenuated immune control of Epstein-Barr virus
891 in humanized mice is associated with the multiple sclerosis risk factor HLA-DR15. Eur J
892 Immunol *51*, 64-75.
893 Zhang, P., Lee, J.S., Gartlan, K.H., Schuster, I.S., Comerford, I., Varelias, A., Ullah, M.A.,
894 Vuckovic, S., Koyama, M., Kuns, R.D.*, et al.* (2017). Eomesodermin promotes the development
895 of type 1 regulatory T (TR1) cells. Sci Immunol *2*.
896

897 **Figure Legends**

898 **Figure 1: Dysregulated Homeostasis of EOMES$^+$Tr1-like effector cells in PwMS**

899 **A.** UMAP of T-cell clusters identified in peripheral blood of treatment-naïve RR-PwMS (n=14)
900 and healthy donors (n=12) by multiparametric flow cytometry. Clusters are identified by
901 numbers, different colors and named as indicated in the panel. **B.** Frequencies among CD4$^+$T-
902 cells, CD69 and Ki67 expression of the indicated T-cell subsets in HDs (n=35) untreated P-
903 PwMS (n=3), treatment-naïve (n=11) and Natalizumab-treated RR-PwMS (n=20). **C.** VLA-4 and
904 CXCR3 expression on CD4$^+$T-cell subsets in treatment-naive RR-MS patients (n=4) and HDs
905 (n=9). **B/C** Statistical significance was calculated by One-way ANOVA.

906

907 **Figure 2: EOMES$^+$Tr1-like cells generate a distinct cluster among single-sequenced CD4$^+$T-**
908 **cells and are enriched and clonally expanded in the cerebrospinal fluid of PwMS**

909 **A.** UMAPs of 13 CD4$^+$T-cell clusters in the blood and the CSF of 4 PwMS. **B.** UMAPs showing
910 EOMES expression in the PB and the CSF of PwMS. **C.** Gene Set Enrichment Analysis of
911 reference EOMES$^+$Tr1-like signature genes of Cluster 7 (Overlay of all conditions). The
912 normalized enrichment score (NES) and its p-value are reported in the panel. **D.** Heatmap of
913 CCR6, GzmK and IL-7R expression in the 13 clusters (Overlay of all conditions). **E.** Heatmap of
914 selected differentially expressed genes of EOMES$^+$Tr1-like cells, CCR6$^+$GzmK$^+$ cells and
915 FOXP3$^+$Tregs. Th17 and Th1 clusters (Cl 4, 8) are shown as controls. Relative average
916 expression levels in the CSF and in the blood of PwMS and control donors are shown. **F.**
917 Frequencies of Cluster 7 (EOMES$^+$Tr1-like) and 11 (CCR6$^+$GzmK$^+$) in the blood and the CSF of
918 PwMs and control donors. Statistical significance was calculated with a paired t-test. **G.**
919 Normalized Shannon's index showing the rate of clonal expansions per cluster in the CSF of
920 PwMS. Higher values reflect lower diversity. Statistical significance was calculated with one-
921 way ANOVA. **H.** TCR clonotype sharings among cells from T-cell clusters analysed in the
922 Heatmap (E) in the blood and the CSF in PwMS and control donors. Statistical significance was
923 calculated with two-way ANOVA. **I.** Frequencies of the indicated CD4$^+$T-cell subsets in
924 peripheral blood (PB, n=17) and the cerebrospinal fluid (CSF, n=5) of treatment-naïve PwMS
925 were assessed by flow cytometry. Statistical significance was calculated with a t-test.

926

927 **Figure 3: EOMES$^+$Tr1-like cells produce high levels of IL-10 in the CSF of PwMS**

928 **A.** UMAPS showing scaled gene co-expression of IL-10 with GzmK (left) or FOXP3 (right). The
929 colour code and the relative scaled co-expression levels are reported in the panel. **B-E.** T-cells
930 in PB and the CSF of untreated PwMS or HDs were activated with PMA and Ionomycin and
931 analyzed for the expression of cytokines and differentiation markers. **B/C.** Clusters were
932 identified and indicated by numbers, colors and names as indicated in the panel**. B.** Relative
933 contributions of the 10 identified clusters to $CD4^+$T-cells in PB and CSF **C.** Diffusion map
934 analysis of the same clusters in PB and CSF predicting differentiation relationships in
935 pseudotime. **D/E.** Analysis of IL-10 producing capacities of $CD4^+$T-cell subsets in the blood of
936 HDs (n=19) and in the blood and the CSF of PwMS (n=4). **D.** IL-10 production by the indicated
937 $CD4^+$T-cell subsets. Statistical significance was calculated by 2-way ANOVA **E.** Pie charts
938 illustrating the relative contributions of the indicated T-cell subsets to the pool of IL-10-
939 producing $CD4^+$T-cells. Color code and mean percentages are reported in the panel. Statistical
940 significance between PB and CSF of PwMS was calculated with a t-test.
941
942 **Figure 4: $EOMES^+$Tr1-like cells are selectively activated by the EBV antigen EBNA1 in PwMS.**
943 **A.** Peripheral blood mononuclear cells were stimulated with peptide pools derived from MOG
944 plus MBP, EBV (immunodominant mix) or JCV (VP1 plus VP2). T-cell subsets were tracked
945 according to differentiation markers, and antigen-specific cells identified by concomitant
946 CD69 upregulation and IFN-γ production (sFigure 7). Frequencies of antigen-specific cells in
947 the indicated subsets are shown as stacked histograms among total $CD4^+$T-cells, according to
948 the indicated color code. Antigen-specific responses were analysed in HDs (MOG/MBP n=12,
949 EBV n=24 and JCV n=10), treatment-naive (n=9, 10 and 8) and Natalizumab-treated PwMS
950 (n=20, 27 and 16). **B.** Antigen-specific $FOXP3^+$Tregs were tracked according to 4-1BB and/or
951 IFN-γ expression among $CD69^+$Tregs (HD n=10-24, untreated RR-PwMS n=2-5, Natalizumab-
952 treated RR-PwMS n=10-15). **C.** CSF-derived $CXCR3^+CCR6^-$"Th1"-cell lines from 5 treatment-
953 naive MS patients were stimulated with EBV or MOG/MBP-derived peptides, and IFN-γ
954 production in $EOMES^+$ and $EOMES^-$ cells analysed. **D.** Antigen-specific IFN-γ responses to
955 overlapping peptide pools derived from EBNA1, BMRF1 and BZLF1 (HD: n=6-10; untreated RR-
956 PwMS: n=2-6; Natalizumab-treated RR-PwMS: n=13-26). **E.** IL-10 production by $EOMES^+$Tr1-
957 like cells and $FOXP3^+$Tregs in response to EBV (immunodominant pool), EBNA1 (n=16) or MOG
958 plus MBP (n=5) in Natalizumab-treated PwMS. **F.** Antigen-specific IFN-γ responses in SLE

959 patients stratified according to CNS involvement (CNS-: n=11, CNS+: n=6) to EBV (upper panel)
960 or EBNA1 (lower panel).
961
962 **Figure 5: EBNA1-specifc EOMES$^+$Tr1-like cells are associated with anti-EBNA1 IgG levels and**
963 **disappear in Ocrelizumab-treated patients.**
964 **A.** Natalizumab-treated PwMS were HLA-haplotyped (Table 3) and the frequencies of EBV- or
965 EBNA1-specific EOMES$^+$Tr1-like cells, Th-cells and FOXP3$^+$Tregs (Figure 4) stratified according
966 to the expression of HLA-DRB1*15:01.**B.** EBNA1-specific EOMES$^+$Tr1-like cells or Th-cells in
967 Natalizumab-treated patients (n=11-19) were plotted against the serum levels of anti-EBNA1
968 IgG antibodies. R and p-values are reported on the right of the panels. **C.** EBV-specific T-cell
969 response in untreated (n (RR, P)=10, 3) and Ocrelizumab-treated PwMS (n(RR, P)=6, 11)).
970 Shown are responses of the indicated EBV-reactive CD4$^+$T-cell subsets and of total CD8$^+$T-cells
971 to EBV (immunodominant pool, upper panels) and to EBNA1 (lower panels). **A/C.** Statistical
972 significances were calculated with an unpaired t-test. **D.** Suppression of CD8$^+$ memory T-cell
973 proliferation induced by EBV-infected B-cells (LCL) and SEB by regulatory T-cell subsets. The
974 proliferation index of CD8$^+$ responder cells alone was set to 1; values of <1 indicate
975 suppression, values >1 help. Naive CD4$^+$T-cells are shown as negative control. Statistics were
976 calculated with a paired t-test.
977
978 **Figure 6: EOMES$^+$ Tr1-like cells produce IL-10 in MS brain lesions.**
979 Triple immunostaining for EOMES (nuclear brown staining), IL-10 (blue) and CD4 (red) reveals
980 presence of EOMES$^+$IL-10$^+$CD4$^+$Tr1-like cells in perivascular immune infiltrates in one active
981 WM lesion (blue/red arrows in A, D-F) and in the inflamed meninges (H) of one MS donor. In
982 the same infiltrates, CD4$^+$ cells expressing only EOMES (red/brown arrow in A and H), EOMES$^-$
983 IL-10$^-$CD4$^+$ cells (red arrow in A) and EOMES$^+$IL-10$^-$CD4$^-$ cells (brown arrow in A and H) were
984 also detected. Panels E and F, inset in D and the left insets in H show four EOMES$^+$IL-10$^+$CD4$^+$
985 cells at high power magnification. In the right inset in H, two EOMES$^-$IL-10$^+$ cells (arrows) one
986 of which co-expresses CD4 (white arrow) are shown at high magnification. Immunostaining
987 for CD8 (B and I) and double staining for CD8 and EOMES (inset in I), performed in serial
988 sections, highlight the presence of numerous CD8$^+$T-cells, some of which express EOMES, in
989 the same immune infiltrates shown in A and H. Immunohistochemistry for CD20 (C and J) and
990 *in situ* hybridization for the small non-coding EBV RNA (EBER) (G, K), performed in consecutive

991 sections, reveal substantial B-cell infiltration and the presence of EBV-infected cells in the
992 same brain areas. Bars: 100 µm in B, C, I-K; 50 µm in G; 20 µm in A, D, H and insets in G and
993 K; 10 µm in E, F and inset in D, right inset in H, and inset in I; 5 µm in the insets in H.

994 **Tables**

995 **Table 1: Characteristics of PwMS and healthy donors**

996

	Healthy Donors	Treatment naive RR-MS	NTZ-treated RR-MS	Untreated P-MS	OCR-treated MS	Untreated MS (OCR Ctr)
Number of subjects	78	13	22	4 (3PP, 1SP)	17 (8 PP, 3 SP, 6 RR)	13 (3 PP, 10 RR)
Female/male (ratio)	47/31 (1.5)	7/6 (1.2)	14/10 (1.4)	0/4 (0)	7/10 (0.7)	5/8 (0.6)
Age, median (range)	34 (20-61)	34 (20-51)	35 (20-62)	48 (28-69)	47 (25-69)	44 (20-69)
EDSS T0, median (range)	n.a.	1.0 (0.0-2.0)	2.0 (1.0-5.5)	2.8 (2.5-4.5)	3.5 (0.0-6.5)	1.0 (0.0-4.5)
EDSS T1 (2023), median (range)	n.a.	1.0 (0.0-2.5)	2.0 (1.0-6.0)	3.0 (2.5-4.5)	3.5 (0.0-7.0)	1.5 (0.0-4.5)

997
998 EDSS: Expanded Disability Status Scale; MS: Multiple Sclerosis; NTZ: Natalizumab; OCR: Ocrelizumab;
999 P: Progressive; PP: Primary Progressive; RR: Relapsing-Remitting; SP: Secondary Progressive
1000
1001 In addition, we collected blood from 17 SLE patients with and without CNS involvement.
1002

1003

1004 **Table 2: Characteristics of SLE patients with and without CNS involvement**

1005

	SLE w/o CNS	SLE CNS
Number of subjects	11	6
Female/male	8/3	6/0
Age, median (range)	41 (21-57)	40 (25-60)
SLEDAI, median (range)	2 (0-8)	4 (0-12)

1006
1007

1008

1009 **Table 3: HLA-DRB1 polymorphisms of Natalizumab-treated PwMS**

Patient	1	2	3	4	5	6	7	8	9	10	11	12	13	14	15	16	17	18	19	20	21	22
HLA-DRB1*	11:04	03:01	01:01	11:01	11:01	13:01	11:04	11:01	11:01	15:01	07:01	13:05	11:04	15:01	13:01	11:01	04:02	04:01	11:01	01:02	11:01	11:01
	13:02	11:04	08:01	13:01	12:01	15:01	15:02	11:01	11:04	16:01	15:01	15:01	15:01	16:01	13:02	13:03	11:01	15:01	16:01	11:04	16:01	15:01

1010

1011 sTable 1: Differentially expressed genes in Cluster 1-13

1012 sTable 2: Differentially expressed genes in EOMES^{+}Tr1-like cells: CSF versus blood

1013 sTable 3: Differentially expressed genes in EOMES$^+$Tr1-like cells versus CCR6$^+$GzmK$^+$ cells

1014 sTable 4: Flow Cytometry antibody panels

1015

1016 **Supplementary Figures**

1017 **sFigure 1: T-cell clusters in peripheral blood of HDs and PwMS identified by multiparametric**
1018 **flow cytometry.**

1019 **A.** Histograms showing the expression of the 18 markers analysed to classify T-cells from
1020 peripheral blood of HDs and of PwMS in the 27 identified T-cell clusters. **B.** UMAP maps of the
1021 identified T-cell clusters showing the individual expression of the 15 most relevant markers.
1022 **C.** Unsupervised hierarchical clustering of the 12 CD4$^+$T-cell clusters according to the
1023 expression of the indicated differentiation markers. Red indicates high and blue low
1024 expression. **D.** Relative contribution of the identified T-cell clusters to the T-cell
1025 compartments in PwMS and HDs

1026

1027 **sFigure 2: Gating strategy to identify pro- and anti-inflammatory EOMES$^+$CD4$^+$T-cell subsets**

1028 **A.** CD4$^+$T-cells were analysed according to the expression of the indicated markers to identify
1029 FOXP3$^+$Tregs (left), GzmB$^+$CTL, Th-cells (central panel) and GzmK$^+$ subsets (right panel),
1030 namely IL-7R$^{+/lo}$Tr1-like and CCR6$^+$ cells. **B.** EOMES expression in the indicated T-cell subsets
1031 (n=9) in PwMS. **C.** Cytokine profiles of GzmK$^+$CD4$^+$T-cell subsets in PwMS

1032

1033 **sFigure 3: Frequencies and activation of CD4$^+$T-cell subsets in PwMS and HDs**

1034 **A.** Frequencies, CD69 and Ki67 expression of the indicated CD4$^+$T-cell subsets in 35 HDs, 3
1035 untreated P-PwMS, 11 treatment-naïve and 20 Natalizumab-treated RR-PwMS. **B.** CXCR3
1036 surface expression on the indicated Ki67$^+$T-cell subsets in the blood of treatment-naïve RR-
1037 PwMS (n=7-11).

1038

1039 **sFigure 4 Annotation of CD4$^+$T-cell clusters.**

1040 **A.** UMAPs of 13 antigen-experienced T-cell clusters in the blood and the CSF of 4 control
1041 donors (with idiopathic intracranial hypertension, IIH). **B.** Dot plot showing expression levels
1042 of the indicated signature genes of central memory, Tfh, Th1, Th2, Th17, CTL, EOMES$^+$Tr1-like,
1043 Treg and IFN-activated cells in the 13 CD4$^+$T-cell clusters **C.** Upper UMAPS: Individual signature

1044 genes of Tfh (Cl1, CXCR5), IFN activate cells (Cl3, IFIT3), Th2 (Cl 10, PTGDR2/CRTH2), CTL (Cl12,
1045 GzmB) and Treg (Cl13, FOXP3). Central UMAPS: Selective expression of EOMES$^+$Tr1-like-
1046 associated signature genes (CHIL2, CCL4, CCR5 and PDCD1 (PD1) in Cluster 7. Lower UMAPS:
1047 Expression of GzmK and of the indicated Th1/17-associated genes in Cl 11(CCR6, RORC, IL-
1048 23R, IL-18RAP). All UMAPS show overlays of all conditions (Blood, CSF, MS, IIH).
1049
1050 **sFigure 5 Features of EOMES$^+$Tr1-like cells in the CSF and the Blood.**
1051 **A.** Heatmaps showing the average expression of genes upregulated in CSF-infiltrating versus
1052 circulating EOMES$^+$Tr1-like cells involved in Cholesterol metabolism and selectively down-
1053 regulated gens in EOMES$^+$Tr1-like cells (upper) and all other CD4$^+$T-cells (lower panel) in the
1054 CSF and in the blood. **B.** Relative contributions of the identified clusters to total antigen-
1055 experienced CD4$^+$T-cells in the blood and the CSF of PwMS and control Donors. **C**. Normalized
1056 Shannon's index showing the rate of clonal expansion per cluster in the PB of PwMS, PB and
1057 CSF of Controls, respectively. Higher values reflect lower diversity. Statistical significance was
1058 calculated with one-way ANOVA. **D**. Bubble plot illustrating the clonal expansion of Treg, Tr1,
1059 CCR6$^+$GzmK$^+$, and CTL in the CSF and PB of PwMS. Bubble radius is proportional to the number
1060 of cells sharing the same TCR within each patient. Clones comprising more than two cells are
1061 annotated with their cell counts. **E.** CXCR3 surface expression in the indicated CD4$^+$T-cell
1062 subsets in peripheral blood (PB, n=11) and in the CSF of PwMS (n=3). Statistical significance
1063 was calculated by One-way ANOVA.
1064
1065 **sFigure 6 Cytokine profiles of CD4$^+$T-cell subsets.**
1066 **A.** UMAPs showing the scaled co-expression of IL-10, IFN-γ and IL-2 with IL-7R. Color code and
1067 relative scaled co-expression levels are reported in the panel. **B**. Hierarchical clustering of the
1068 10 identified CD4$^+$ T-cell clusters according to the expression of cytokines and differentiation
1069 markers in the blood and CSF of active MS patients. **C.** Diffusion Maps showing the expression
1070 of 7 principal markers that characterize the cytokine producing T-cell clusters. **D.** IL-
1071 production by EOMES$^+$Tr1-like cells in HDs (n=19) and RR- (n=2-3) or P-PwMS (PB n=2) in the
1072 blood or the CSF. **E.** Analysis of IFN-γ producing capacities of CD4$^+$T-cell subsets in the blood
1073 of HDs (n=19) and in the blood and the CSF of PwMS (n=4).
1074
1075 **sFigure 7: Assessment of antigen-specific T-cell subsets *ex vivo.***

1076 **A.** TCR-induced T-cell responses identified by concomitant CD69 and IFN-γ induction in gated
1077 $CD4^+$T-cells. **B.** TCR-induced responses of $FOXP3^+$Tregs identified by concomitant CD69 and
1078 4-1BB induction. **C.** TCR-induced upregulation of CD40L versus IL-10 on total $CD4^+$T-cells.
1079 **A-C.** Shown are the negative (Ctr-, no antigen) and the positive (Ctr+, super-antigen SEB)
1080 control. **D.** Stable expression of subset-specific markers in unstimulated (Ctr-) and SEB-
1081 stimulated (Ctr+) $CD4^+$T-cells. **E** Representative stainings showing $CD69^+$IFN-γ^+ cells following
1082 stimulation with EBV- but not with MOG/MPB-derived peptides. **F**. Five untreated PwMS were
1083 stimulated with the immunodominant pool of EBV peptides (EBV) and EBV-specific $CD4^+$ and
1084 $CD8^+$T-cells tracked by CD69 and IFN-γ co-expression. Shown are three technical triplicates for
1085 each patient (PT). The mean coefficients of variance (CV) and the intraclass correlation
1086 coefficients (ICC) are indicated. **G**. Right: Proliferation of FACS-purified T-cell subsets from
1087 healthy donors following stimulation with autologous monocytes and EBV-derived peptides
1088 for 7 days according to CellTrace dilution. Shown is one representative Histogram of
1089 proliferating Tr1-cells (purified as CD4+$CCR5^+PD1^+CD27^+CCR6^-$), bars show mean proliferation
1090 of 3 HDs. Right: Cell $Trace^-$ $CD4^+$T-cells were analysed for GzmK and EOMES expression.
1091
1092 **sFigure 8 Antigen specificities of individual T-cell subsets.**
1093 **A**. Antigen specificities of T-cell subsets. Reported are frequencies $CD69^+$IFN-γ^+ cells in
1094 individual $CD4^+FOXP3^-$T-cell subsets among $CD4^+$T-cells and responses in total $CD8^+$T-cells in
1095 HDs (n=10-21), in untreated (n=10-14) and Natalizumab-treated PwMS (n=17-20). Left panels
1096 show responses following stimulation with overlapping peptide pools of MOG and MBP,
1097 central panels to an immunodominant peptide pool derived from EBV or and right panels to
1098 overlapping peptide pools of VP1 and VP2 from JCV. Squares on top of columns indicate
1099 statistical significances as compared to the no peptide control. Stars on top of lines indicate
1100 statistical significances between different cohorts. **B.** Lack of responses of $GzmK^+$T-cell
1101 subsets, i.e. frequencies of $CD69^+$IFN-γ^+ cells in the indicated subset among total $CD4^+$T-cells,
1102 to PLP (6 HDs and 6 Natalizumab-treated MS patients) **C.** $CD4^+CXCR3^+CCR6^-$"Th1" and $CXCR3^-$
1103 $CCR6^+$"Th17" cell lines derived from the CSF from 5 different treatment-naïve MS patients
1104 were analysed for EOMES expression. Shown are the mean percentages of $EOMES^+$ cells, and
1105 the p-value is indicated.
1106

1107 **sFigure 9 Specificities of individual T-cell subsets for latent or lytic EBV antigens.**

1108 **A.** Responses of the indicated T-cell subsets to individual EBV-derived antigens, namely
1109 EBNA1, BZLF1 and BMRF1 in HDs (EBNA1: n=9, BZLF1: n=6, BMRF1: n=7), untreated ("MS",
1110 EBNA1: n=9, BZLF1: n=8, BMRF1: n=3 and Natalizumab-treated PwMS ("+NTZ" EBNA1: n=19,
1111 BZLF1: n=17, BMRF1: n=11). Responses of FOXP3$^+$Tregs (HD: n=7, MS n=3, +NTZ: n=11) were
1112 assessed according to CD69 and 4-1BB up-regulation and/or IFN-γ production, all other
1113 subsets according to CD69 up-regulation and concomitant IFN-γ production. Squares on top
1114 of columns indicate statistical significances as compared to the no peptide control. Stars on
1115 top of lines indicate statistical significances between different cohorts. **B.** Sorted Tr1-like
1116 cells, Th1-cells or Tregs from a PwMS were labelled with CellTrace, stimulated with
1117 autologous monocytes and EBNA1 peptides and proliferation and CD25 expression analysed
1118 after 7 days. **C.** IL-10 production by Th-cells in response to EBV, EBNA1 and MOG/MBP in
1119 Natalizumab-treated PwMS (n=12).

1120

1121 **sFigure 10 Specificities of individual T-cell subsets for EBV antigens in SLE patients stratified**
1122 **according to CNS involvement.**

1123 **A.** IFN-γ responses of peptide-activated CD4$^+$GzmK$^+$T-cell subsets, CD4$^+$CTL, Th-cells and
1124 FOXP3$^+$Tregs to EBV and EBNA1 in SLE patients without (CNS -, n=11) or with (n=6) CNS
1125 involvement ("CNS +"). **B.** IL-10 production in EBV and EBNA1-activated EOMES$^+$Tr1-like cells
1126 and by FOXP3$^+$Tregs in SLE patients with and without CNS involvement.

1127

1128 **sFigure 11 Associations of EBNA1-specific T-cells with MS risk factors.**

1129 **A.** IL-10 production by EOMES$^+$Tr1-like cells and FOXP3$^+$Tregs, in response to EBV and EBNA1
1130 in PwMS stratified according to HLA-DRB1*15:01 expression. **B.** Anti-EBNA1 IgG serum levels
1131 in HDs (n=15) and MS patients (untreated: n=15, Natalizumab-treated: n=21). **C-E:** Regression
1132 analysis of EBNA1-specific T-cell population with anti-EBNA1 IgG levels. R- and p-values are
1133 indicated. **C.** shows IFN-γ-producing EBNA1-specific cells among total CD4$^+$ and CD8$^+$T-cells.
1134 **D.** shows EBNA1-specific FOXP3$^+$Tregs expressing 41-BB. **E.** shows EBNA1-specific Th-cells
1135 expressing CD40L. **F**. CD40L up-regulation of CD4$^+$T-cell stimulated with EBV- or EBNA1-
1136 derived peptides T-cells (n=13). Statistical significance of CD40L expression of Th-cells versus
1137 Tr1-cells and Tregs was calculated by two-way Annova.

1138

1139 **sFigure 12: Impact of $CD4^+$T-cell subsets on the proliferation of $CD8^+$ memory T-cells**
1140 **stimulated with EBV-infected B-cells.**

1141 FACS-purified $CD8^+CD45RA^-$ memory T-cells were labelled with CellTrace and stimulated with
1142 EBV-infected B-cells (LCL) and SEB. Shown are the Cell Trace histograms after 7 days in the
1143 absence or presence of the indicated $CD4^+$T-cell subsets of a representative experiment. The
1144 Proliferation indices and the percentage of undivided cells (highlighted in grey) are reported.

1145

1146 **sFigure 13 Negative control for EOMES and IL-10 staining in brain sections.**

1147 Triple immunohistochemistry in bright field of MS brain tissue stained with 5 µg/ml purified
1148 rat IgG1 k isotype control (eBRG1), 5 µg/ml purified mouse IgG1k isotype control (P3.6.2.8.1)
1149 (both by Thermo Fisher Scientific) and rabbit monoclonal antibody to CD4, performed as
1150 described. Only immunoreactivity for CD4+ cells (red) was observed. Bar = 100 µm.

1151

Marker	Fluorochrome	Clone	Brand	cat. N°	Dilution
IL-7R	BB700	HIL-Ti7R-M21	BD	566398	30
CXCR3	PE-Cy7	1C6/CXCR3	BD	560831	60
CCR6	BUV496	11A9	BD	612948	30
CD4	BUV563	SK3	BD	612912	180
CD8	BUV805	SK1	BD	564912	200
L/D dye	*FVS780*	/	*BD*	*565388*	*200*
CD45RA	BV605	HI100	BD	562886	140
CD69	BV786	FN50	BD	563834	100
/	/	/	/	/	/
CD3	BUV737	UCHT1	BD	612750	140
CCR7	PE-CF594	150503	BD	562381	60
CD161	PE-Cy5	DX12	BD	551138	40
CD25	APC-R700	2A3	BD	565106	40
CD27	BV480	L128	BD	566139	120
PD-1	BV650	EH12.1	BD	564104	30
CCR5	BUV395	2D7/CCR5	BD	565224	30
FOXP3	Alexa Fluor488	259D	BioLegend	320212	50
GzmK	PE	GM6C3	SantaCruz	SC56125	100
Eomes	eFluor 660	WD1928	Invitrogen	50-4877-42	25
GzmB	BV421	GB11	BD	563389	80
Ki-67	BV711	B56	BD	563755	80
IFN-γ	BV750	B27	BD	566357	140

Marker	Fluorochrome	Clone	Brand	cat. N°	Dilution
IL-7R	BB700	HIL-Ti7R-M21	BD	566398	30
CXCR3	PE-Cy7	1C6/CXCR3	BD	560831	60
CCR6	BUV496	11A9	BD	564659	30
CD4	BUV563	SK3	BD	566000	180
CD8	BUV805	SK1	BD	564912	200
L/D dye	*FVS780*	/	*BD*	*565388*	*200*
CD107a	BV605	H4A3	BioLegend	328634	40
CD49d	BV786	9F10	BD	744588	120
CD29	BUV661	38047	BD	750084	60
CD69	BUV737	FN50	BD	612817	40
T-bet	PE-CF594	O4-46	BD	562467	40
CD40L	PE-Cy5	24-31	BioLegend	310808	50
IL-17A	APC-R700	N49-653	BD	565163	30
IL-2	BV510	5344.111	BD	563265	40
41-BB	BV650	H4A3	BioLegend	328637	40
TNFα	BUV395	MAb11	BD	563996	160
FOXP3	AlexaFluor488	259D	BD	320212	50
GzmK	PE	GM6C3	SantaCruz	SC56125	100
Eomes	eFluor 660	WD1928	Invitrogen	50-4877-42	25
GzmB	BV421	GB11	BD	563389	80
Ki-67	BV711	B56	BD	563755	80
IFN-γ	BV750	B27	BD	566357	140

Marker	Fluorochrome	Clone	Brand	cat. N°	Dilution
IL-7R	BB700	HIL-Ti7R-M21	BD	566398	30
CCR6	BUV496	11A9	BD	564659	30
L/D dye	*FVS780*	/	*BD*	*565388*	*200*
CD8	BUV805	SK1	BD	564912	200
CD4	BUV563	SK3	BD	566000	180
FOXP3	AF488	259D	BD	320212	50
GzmB	BV421	GB11	BD	563389	80
IFN-γ	BV750	B27	BD	566357	140
IL-17A	APC-R700	N49-653	BD	565163	30
Eomes	PE-Cy7	WD1928	Invitrogen	25-4877-42	30
GzmK	AlexaFluor647	G3H69	BD	566655	40
CD40L	BV605	24-31	BioLegend	310825	40
IL-10	PE	JES3.9D7	BioLegend	501404	30
GM-CSF	PECF594	BVD2-21C11	BioLegend	562857	30

Figure 1

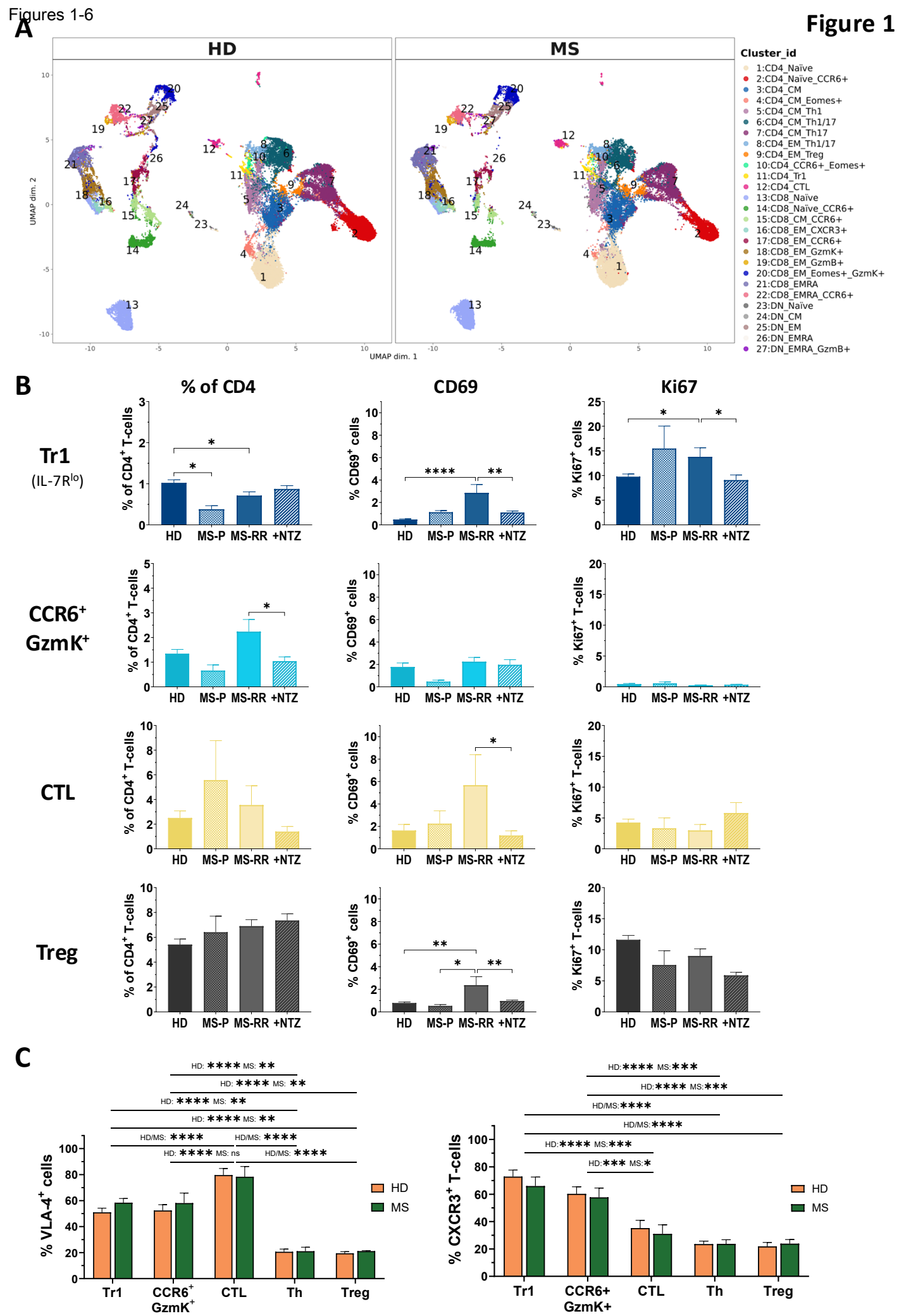
A
HD
MS
UMAP dim. 1
UMAP dim. 2
Cluster_id
1:CD4_Naïve
2:CD4_Naïve_CCR6+
3:CD4_CM
4:CD4_CM_Eomes+
5:CD4_CM_Th1
6:CD4_CM_Th1/17
7:CD4_CM_Th17
8:CD4_EM_Th1/17
9:CD4_EM_Treg
10:CD4_CCR6+_Eomes+
11:CD4_Tr1
12:CD4_CTL
13:CD8_Naïve
14:CD8_Naïve_CCR6+
15:CD8_CM_CCR6+
16:CD8_EM_CXCR3+
17:CD8_EM_CCR6+
18:CD8_EM_GzmK+
19:CD8_EM_GzmB+
20:CD8_EM_Eomes+_GzmK+
21:CD8_EMRA
22:CD8_EMRA_CCR6+
23:DN_Naïve
24:DN_CM
25:DN_EM
26:DN_EMRA
27:DN_EMRA_GzmB+
B
% of CD4
CD69
Ki67
Tr1
(IL-7R^{lo})
CCR6$^+$ GzmK$^+$
CTL
Treg
% of CD4$^+$ T-cells
% CD69$^+$ cells
% Ki67$^+$ cells
% Ki67$^+$ T-cells
HD
MS-P
MS-RR
+NTZ
C
% VLA-4$^+$ cells
HD: **** MS: **
HD: **** MS: **
HD: **** MS: **
HD: **** MS: **
HD/MS: ****
HD/MS: ****
HD: **** MS: ns
HD/MS: ****
% CXCR3$^+$ T-cells
HD:**** MS:***
HD:**** MS:***
HD/MS:****
HD/MS:****
HD:**** MS:***
HD:*** MS:*
Tr1
CCR6$^+$ GzmK$^+$
CTL
Th
Treg
HD
MS

Figure 2

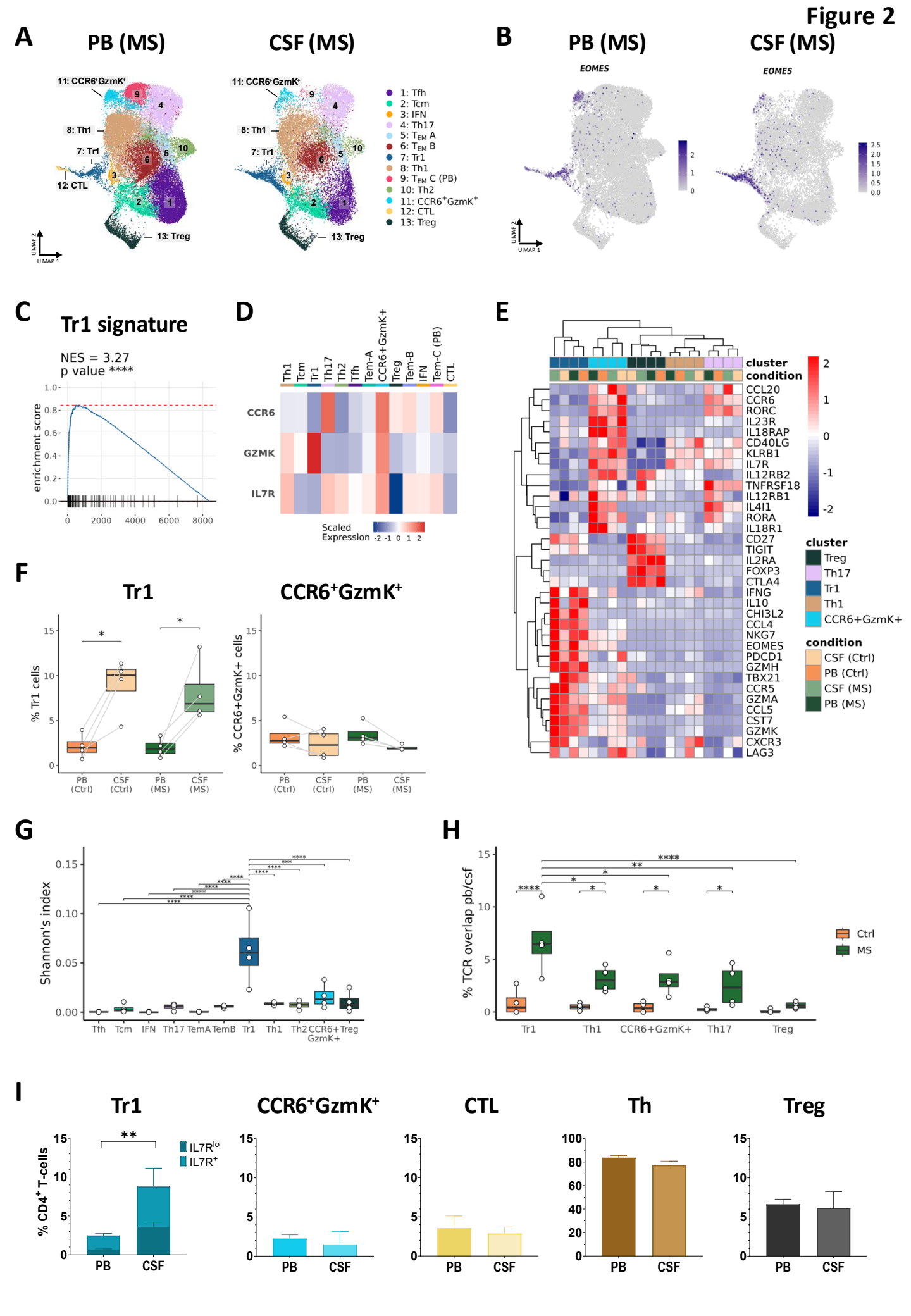
A
PB (MS)
CSF (MS)
11: CCR6+GzmK+
8: Th1
7: Tr1
12: CTL
13: Treg
1: Tfh
2: Tcm
3: IFN
4: Th17
5: TEM A
6: TEM B
7: Tr1
8: Th1
9: TEM C (PB)
10: Th2
11: CCR6+GzmK+
12: CTL
13: Treg
UMAP 1
UMAP 2
B
PB (MS)
CSF (MS)
EOMES
C
Tr1 signature
NES = 3.27
p value ****
enrichment score
D
Th1
Tcm
Tr1
Th17
Th2
Tfh
Tem-A
CCR6+GzmK+
Treg
Tem-B
IFN
Tem-C (PB)
CTL
CCR6
GZMK
IL7R
Scaled Expression
E
cluster
condition
CCL20
CCR6
RORC
IL23R
IL18RAP
CD40LG
KLRB1
IL7R
IL12RB2
TNFRSF18
IL12RB1
IL4I1
RORA
IL18R1
CD27
TIGIT
IL2RA
FOXP3
CTLA4
IFNG
IL10
CHI3L2
CCL4
NKG7
EOMES
PDCD1
GZMH
TBX21
CCR5
GZMA
CCL5
CST7
GZMK
CXCR3
LAG3
Treg
Th17
Tr1
Th1
CCR6+GzmK+
CSF (Ctrl)
PB (Ctrl)
CSF (MS)
PB (MS)
F
Tr1
CCR6+GzmK+
% Tr1 cells
% CCR6+GzmK+ cells
PB (Ctrl)
CSF (Ctrl)
PB (MS)
CSF (MS)
G
Shannon's index
Tfh
Tcm
IFN
Th17
TemA
TemB
Tr1
Th1
Th2
CCR6+ GzmK+
Treg
H
% TCR overlap pb/csf
Tr1
Th1
CCR6+GzmK+
Th17
Treg
Ctrl
MS
I
Tr1
CCR6+GzmK+
CTL
Th
Treg
% CD4+ T-cells
IL7Rlo
IL7R+
PB
CSF

Figure 3

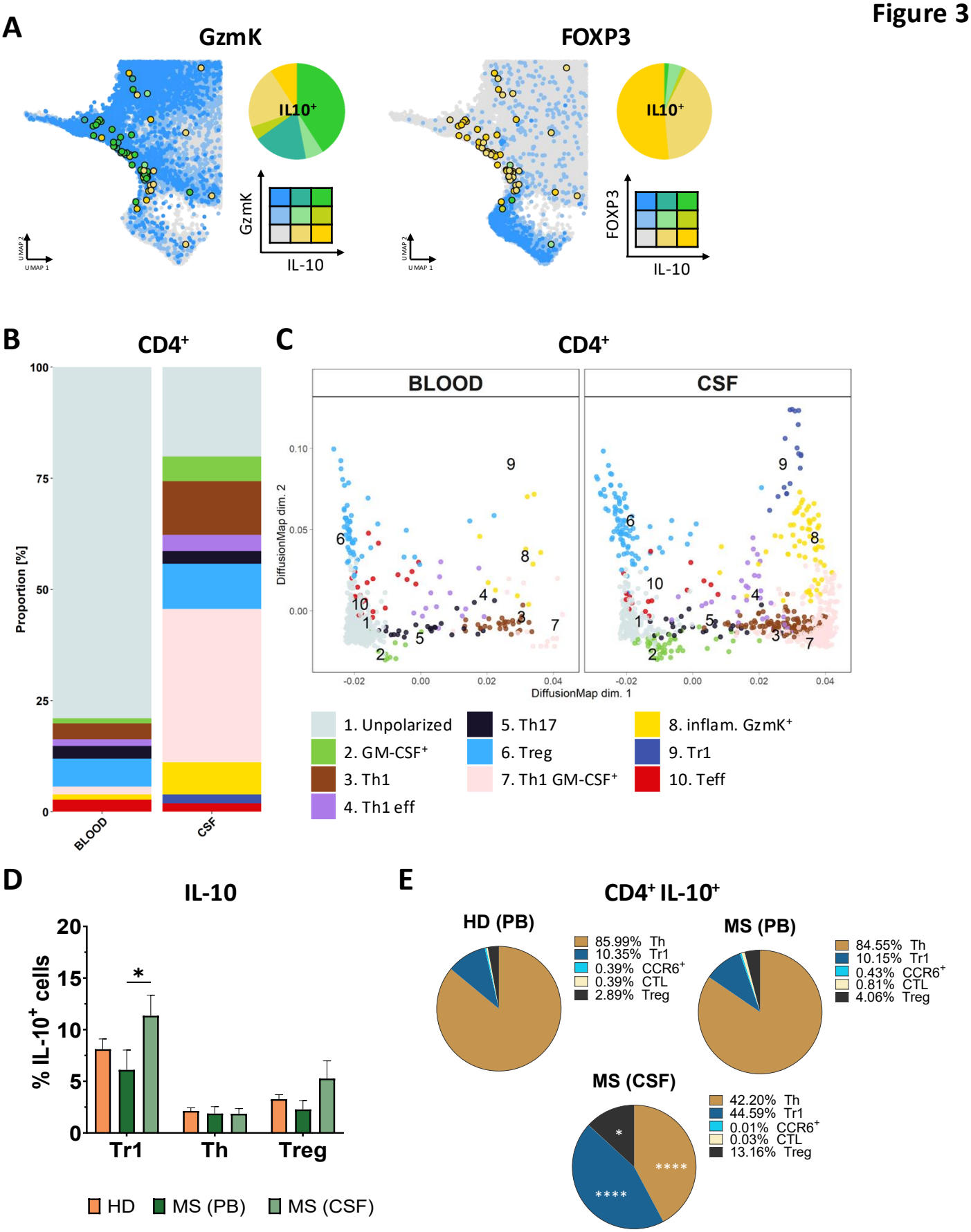
A
GzmK
FOXP3
IL10+
GzmK
IL-10
FOXP3
UMAP 1
UMAP 2
B
CD4+
Proportion [%]
BLOOD
CSF
C
CD4+
BLOOD
CSF
DiffusionMap dim. 1
DiffusionMap dim. 2
1. Unpolarized
2. GM-CSF+
3. Th1
4. Th1 eff
5. Th17
6. Treg
7. Th1 GM-CSF+
8. inflam. GzmK+
9. Tr1
10. Teff
D
IL-10
% IL-10+ cells
Tr1
Th
Treg
HD
MS (PB)
MS (CSF)
E
CD4+ IL-10+
HD (PB)
85.99% Th
10.35% Tr1
0.39% CCR6+
0.39% CTL
2.89% Treg
MS (PB)
84.55% Th
10.15% Tr1
0.43% CCR6+
0.81% CTL
4.06% Treg
MS (CSF)
42.20% Th
44.59% Tr1
0.01% CCR6+
0.03% CTL
13.16% Treg

Figure 4

A

MOG/ MBP

EBV

JCV

CD4

%antigen-specific CD4+

Th ***

Tr1 ****/*

Tr1 **/ns

Th **

Th *

***

HD MS +NTZ

Treg
Th
CTL
CCR6+GzmK+
Tr1 IL-7R+
Tr1 IL-7Rlo

B

Treg

%antigen-specific Tregs

*
4-1BB

***
4-1BB

**
4-1BB

*
4-1BB

IFN-γ
4-1BB IFN-γ
4-1BB
Paired t-test vs Ctr-

C

Th1-lines (CSF, MS)

% IFN-γ+ cells

*

* **

CTR -
EBV
MOG/ MBP

Tr1 (EOMES+)

Th1 (EOMES-)

D

EBNA1 (latent)

BMRF1 (lytic)

BZFL1 (lytic)

% antigen-specific CD4+

Th ****

Th **

Th **

HD MS +NTZ

Treg
Th
CTL
CCR6+GzmK+
Tr1 IL-7R+
Tr1 IL-7Rlo

E

IL-10

Tr1

‰IL-10+ cells

*

*

-
EBV
EBNA1
MOG-MBP

Treg

**

**

F

SLE

EBV (Pool)

EBNA1

% antigen-specific CD4+

CNS-
CNS+

Treg
Th
CTL
CCR6+GzmK+
Tr1 IL-7R+
Tr1 IL-7Rlo

Figure 5

A

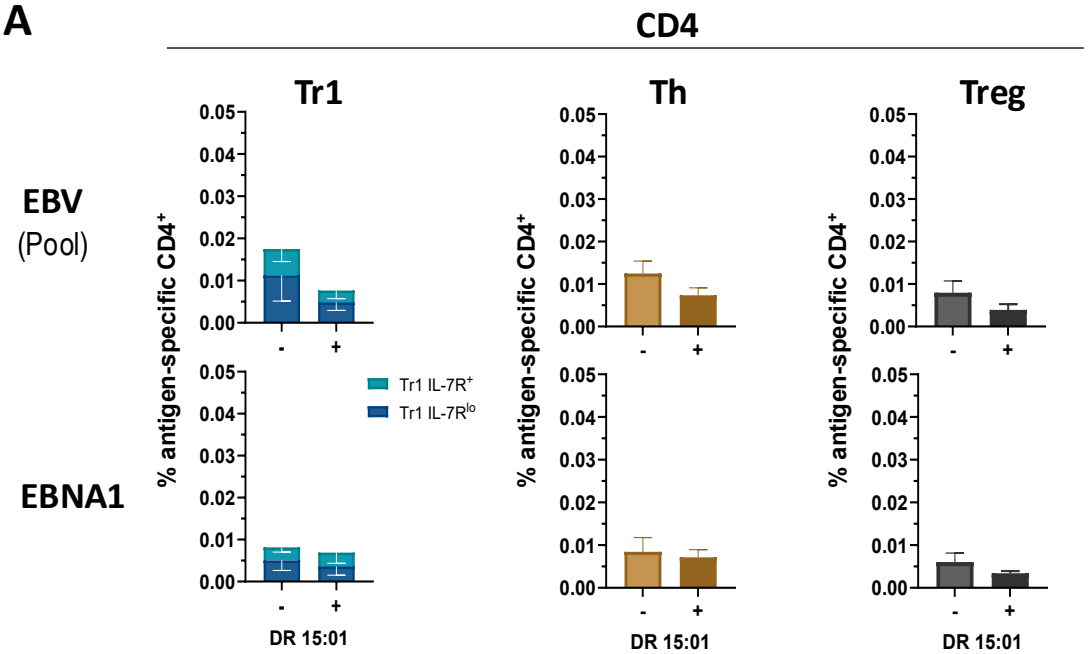

B

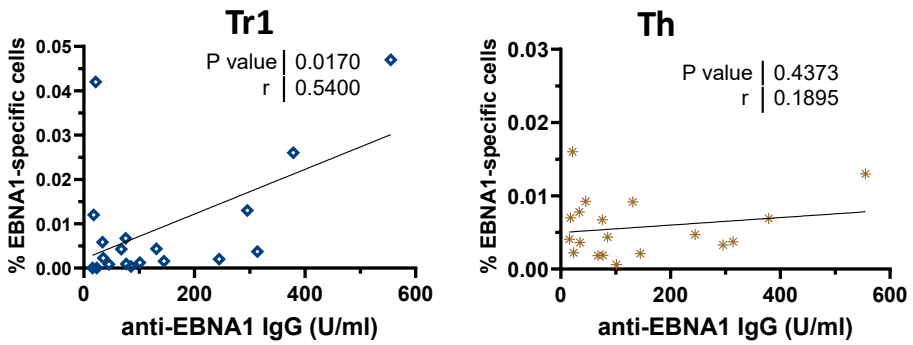

C

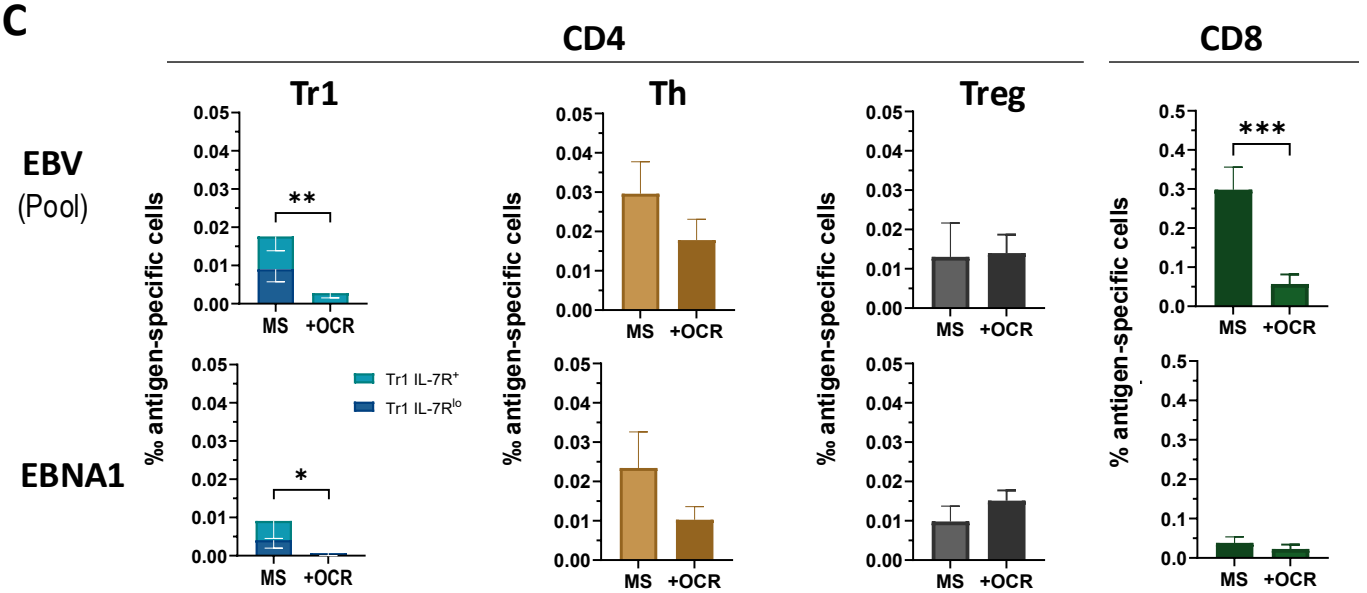

D

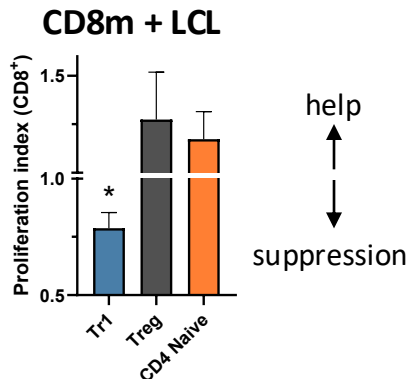

Figure 6

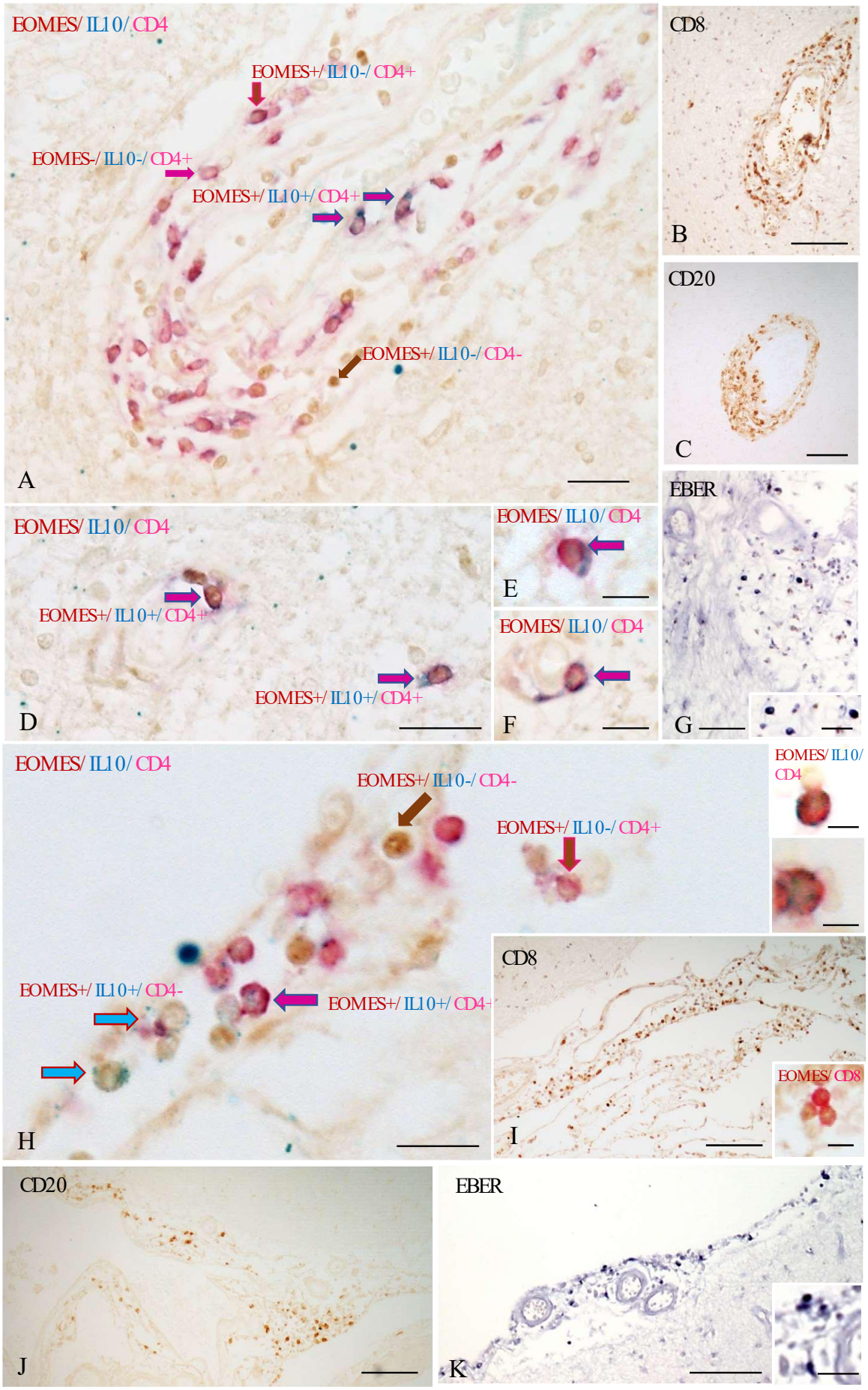
EOMES/ IL10/ CD4
EOMES+/ IL10-/ CD4+
EOMES-/ IL10-/ CD4+
EOMES+/ IL10+/ CD4+
EOMES+/ IL10-/ CD4-
A
CD8
B
CD20
C
EBER
G
EOMES/ IL10/ CD4
EOMES+/ IL10+/ CD4+
EOMES+/ IL10+/ CD4+
D
EOMES/ IL10/ CD4
E
EOMES/ IL10/ CD4
F
EOMES/ IL10/ CD4
EOMES+/ IL10-/ CD4-
EOMES+/ IL10-/ CD4+
EOMES+/ IL10+/ CD4-
EOMES+/ IL10+/ CD4-
H
EOMES/ IL10/ CD4
CD8
EOMES/ CD8
I
CD20
J
EBER
K